JOURNAL OF MATERIALS SCIENCE 19 (1984) 1043–1076

Review
The status of rapid solidification of alloys in research and application

H. JONES
Department of Metallurgy, University of Sheffield, Sheffield S1 3JD, UK

The status of rapid solidification is discussed in terms of recent progress in modelling methods of achieving solidification at high cooling rates and its effects on alloy constitution and microstructure. Applications currently in view are reviewed under the following headings: high-strength structural materials; tool and bearing materials; high-temperature materials, corrosion-resistant, catalytic and storage materials; and electrical and magnetic materials. It is concluded that the future of rapid solidification is not identifiable with any one process, activity or application and that many unresolved questions remain to challenge both the scientific and business communities.

1. Introduction

Solidification is the process of formation of solid. Metallic materials can be solidified by electro- or electroless-deposition from salt solution, by vapour or sputter deposition, as well as by freezing of their melts. Deposition from salt solution is highly system-specific and slow ($\sim 0.1\,mm\,h^{-1}$ is considered [1] to be a high rate of electrodeposition). Vapour and sputter deposition, although very widely applicable, are also slow (even high-rate sputtering gives a deposition rate of no more than $20\,\mu m\,h^{-1}$ [2]). Solidification from the melt is widely applicable and also allows solid to form comparatively rapidly. Even the slowest steady state crystal growth from the melt is carried out at rates of $\sim 1\,mm\,h^{-1}$ and a typical steel ingot will freeze in its cast iron mould at an average rate of $\sim 100\,mm\,h^{-1}$. On this basis even *normal* solidification from the melt, as carried out by established processes in industry year in and year out, is not slow. What then, do we mean by "rapid" solidification from the melt?

This question is perhaps best answered by reference to the "gun" technique of splat cooling, introduced by Pol Duwez [3, 4] some 20 years ago, in which a shock wave atomizes a small molten charge and propels the resulting droplets at sonic velocity to form a "splat", of non-uniform thickness varying from $\sim 50\,\mu m$ to $< 0.1\,\mu m$, on impact with a rigid chill surface. Measurements indicate cooling rates of at least 10^5 to $10^6\,K\,sec^{-1}$ with estimates as high as $10^{10}\,K\,sec^{-1}$ for the thinnest regions. This compares with cooling rates no higher than $100\,K\,sec^{-1}$ associated with solidification in conventional processing, typical cooling rates being about 10^{-1} to $10^{-2}\,K\,sec^{-1}$, the lowest values being 10^5 to $10^{-6}\,K\,sec^{-1}$ for very large sand castings.

What is different when solidification is carried out at such high cooling rates? One difference is that it is possible to achieve relatively large (hundreds of degrees) supercooling of the melt before significant amounts of solid phase can form. This can result in *constitutional* changes in that retained equilibrium phases can have compositions outside their equilibrium limits (*solid solubility extension*), or that non-equilibrium phases can form as a result of being favoured kinetically over equilibrium phases. Formation of eutectic cementite rather than graphite in chilled cast irons is a rare example of such an effect occurring at supercoolings of only a few degrees. Such effects become the rule rather than the exception when cooling rates exceed $10^6\,K\,sec^{-1}$. Resulting non-equilibrium phases may be crystalline or glassy (non-crystalline) and maintainence of a high cooling rate following their formation helps to ensure their retention to ambient tem-

0022–2461/84 $03.00 + .12 © *1984 Chapman and Hall Ltd.*

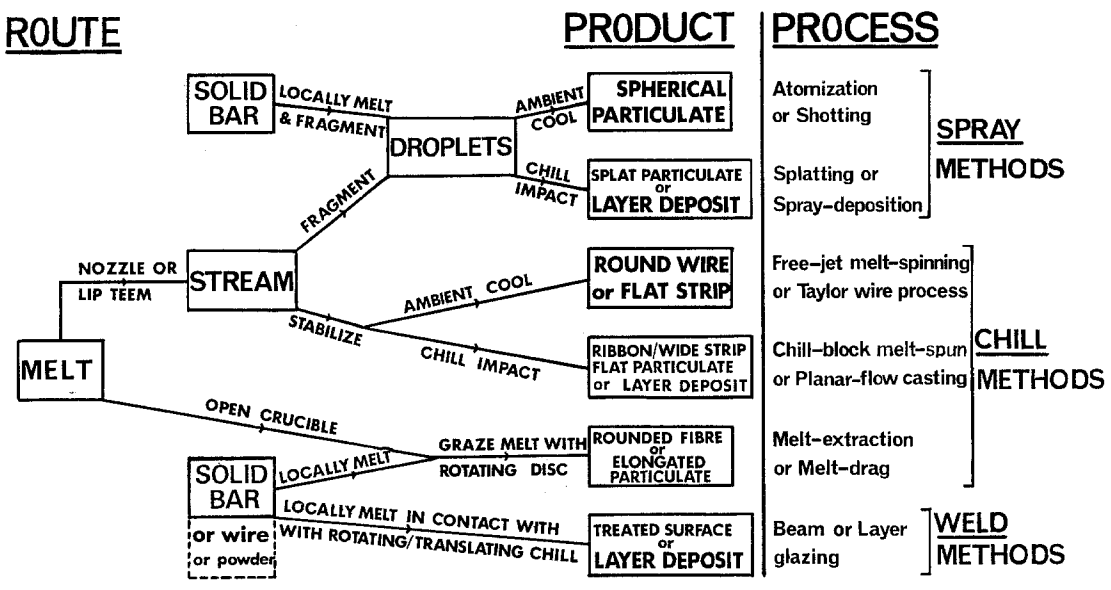

Figure 1 Some production routes for RSR-processing and their products [5].

perature. Glass formation was previously restricted to melts such as those of oxides from which crystallization is particularly sluggish, but availability of cooling rates $> 10^6$ K sec^{-1} has facilitated glass formation even from readily-crystallizing metallic melts, establishing a new class of material, the *metallic glasses*. These have been the object of a major new research and development activity, particularly in the last decade, including a continuing search for commercial applications. A second difference is that shortening of diffusion distances and formation times results in substantial refinement and re-morphologizing of microstructure both for matrix and minor phases. This has important consequences for conventional alloys limited in processability and/or service performance by formation at the ingot stage of non-uniform distributions of coarse subsidiary phases and segregates. The resulting possibilities for more effective use of alloy additions and of processing options are the origin of present burgeoning efforts to establish rapid-solidification-rate (RSR) processing* as a reliable means of manufacturing high quality, more economical products with improved combinations of properties.

The purpose of this article is to provide an overview of the status of RSR-processing, both as a means of attaining structural states of interest for advancing understanding of materials behaviour and as a means of production for commercial application. This will be done under the three headings of Principles, Effects and Applications. Further details on specific aspects can be obtained in a recent monograph [5] and via the compendia and specialized review articles referred to therein.

2. Principles

Achievement of cooling rates in the range 10^2 to 10^{10} K sec^{-1} is dependent on rapid formation of a sufficiently small dimension of cross-section in good contact with an effective heat sink. For effectively perfect contact conditions between metallic melt and chill surface, standard heat flow analyses predict cooling rate ϵ at the uncooled boundary equal to B/z^2, where B is a function of relevant temperature intervals and materials properties and has a value $\sim 10^4$ mm^2 K sec^{-1} [6]. Thus, unit section dimension z must not exceed 10 mm, 0.1 mm and 10 μm respectively if cooling rates of 10^2, 10^6 and 10^{10} K sec^{-1} are to be achieved. The magnitude of heat transfer coefficient h at the chilled boundary required to ensure effectively perfect contact is $\gtrsim K/z$, where K is the conductivity of solidified melt or chill surface material, so that the need to ensure good thermal contact becomes increasingly important with increase of desired cooling rate and thus decrease of required z.

Alternative routes for achieving high cooling rate during, and preferably following, solidification (Fig. 1) thus all have in common the basic require-

*RSR = Rapid Solidification Rate; RSP = Rapidly Solidified Powder or Rapid Solidification Processing; RST = Rapid Solidification Technology.

ments to rapidly produce a section of small z under conditions of sufficiently high h. Methods involving droplet formation (spray methods) which include the "gun" technique, are the most complex, usually involving three stages: stream formation, fragmentation and cooling. The rotary atomization technique of making RSR powders developed by Pratt and Whitney [8] has been a major stimulus, parallel developments including ultrasonic [9] and electrodynamic [10] methods of droplet formation. Attention has also been given to building-up of thick rapidly-solidified deposits by successive impact of incident droplets, thereby combining rapid solidification with an element of consolidation in a single operation [11–13]. *Chill* methods instead generally involve stabilizing any stream formed to generate a continuous or semi-continuous filament or thin strip. Particular attention has been given to chill-block melt-spinning (CBMS) [14] and planar-flow casting (PFC) [15] methods developed as RSR-processes by Allied Corporation and widely adopted by others. Planar-flow casting and the related Battelle processes of melt-drag [16] and melt-extraction [17] form their products essentially without formation of a stream and, in the latter case, even without the need for melt to flow through an orifice, so are among the most direct of available routes from melt to product. *Weld* methods of directed-energy processing [18] take this trend a stage further by melting *in situ* at the chill surface, rather than in a crucible, so giving an RSR-treated surface or a thick layer deposit on a suitable former. The potential of this hitherto neglected technology is now receiving due attention over a relatively broad front.

Modelling of this range of processing methods involves taking into account both fluid-dynamic and heat transfer aspects. Fluid dynamics governs the size distribution and velocity of droplets produced by fluid-driven and rotary atomization and also the amount of spreading and thinning of such droplets that occurs on impact with a chill surface. For the relatively well-defined situation of direct-drop formation at the rim of a rotating disc at low feed rates, droplet size is determined by the balance between the generating effect of centrifugal force ($= V\rho\omega^2 D/2$) and the restraining effect of surface tension force ($\propto \gamma d$) where respectively V and d are droplet volume ($\pi d^3/6$) and diameter, ω and Δ are disc speed of rotation and diameter and ρ and γ are liquid density and surface tension giving [19]

$$d = (a/\omega)(\gamma/\rho\Delta)^{1/2} \quad (1)$$

where a is expected to be close to 4 as confirmed experimentally for a variety of liquids including some liquid metals. Increased feed rate gives first ligament and then sheet formation [20] prior to breakdown into droplets (Fig. 2). This more complex situation and the corresponding one for fluid-driven atomization is difficult to model realistically and so recourse has been made to empirical relationships such as that of Lubanska [21] (Fig. 3) for fluid atomization of liquid metals and wax:

$$d = (a/v)[\gamma\phi\alpha(1+\beta)/\rho_0]^{1/2} \quad (2)$$

where ϕ is melt orifice or stream diameter, ρ_0 and

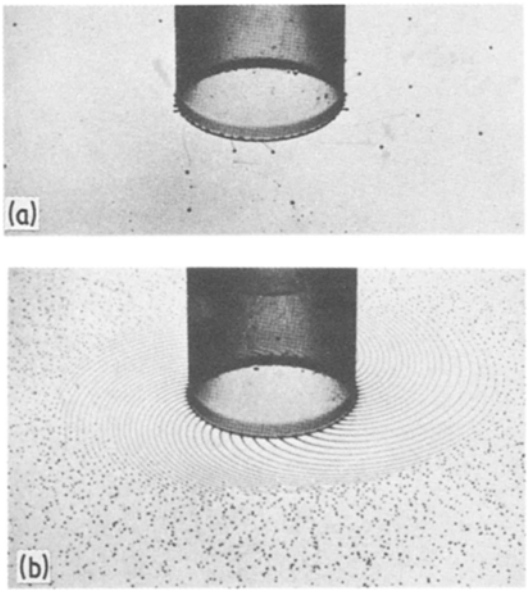

Figure 2 Showing transition from (a) direct to (b) prior ligament to (c) prior sheet formation of droplets with increasing feed rate (1 to 8 to 45 kg h^{-1}) in rotary atomization [20].

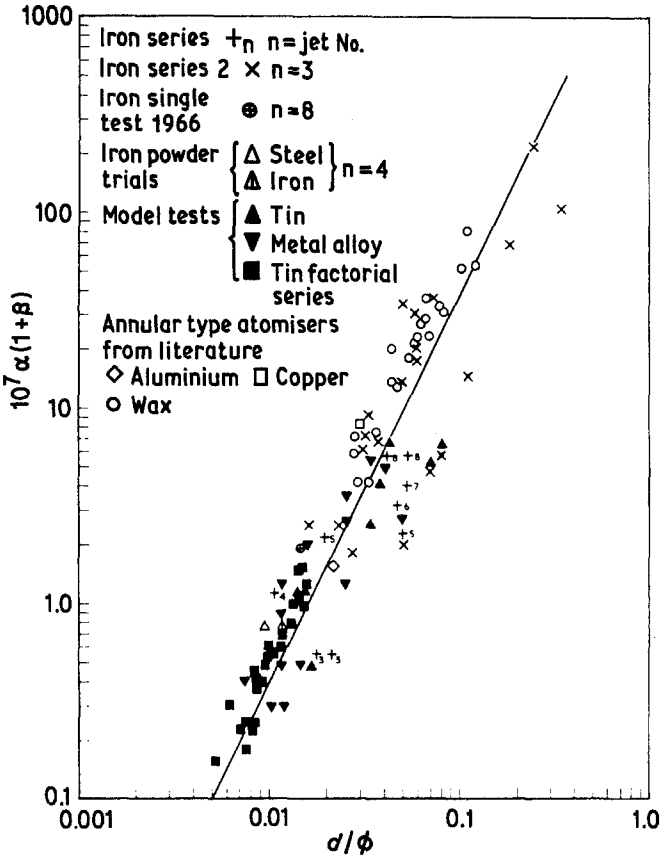

Figure 3 Showing $10^7\alpha(1 + \beta)$ as a function of d/ϕ for gas-jet atomization of liquid metals and wax [21].

v are density and relative velocity of atomizing fluid, α and β are ratios of kinematic viscosity and mass flow rate, respectively, of the melt of those of the atomizing fluid, and a is ~ 50. A problem in applying this relationship is that relative velocity v must be known at the point of atomization. When this was determined, a recent study [22] at Sheffield showed excellent agreement between measured mean droplet size and the predictions of Equation 2. Heat transfer from atomized droplets during travel subsequent to their formation has been the subject of recent analyses [23–25]. These predict the extent to which solidification kinetics are accelerated in the presence of bulk supercooling within the solidifying droplet. At least the initial solidification then takes place at a rate governed by the recalescence into the undercooled liquid of latent heat released at the solidification front, which thus advances into the melt under the influence of a negative temperature gradient. The predictions [24] indicate that the expected magnitude of external heat transfer coefficient at the droplet surfaces has little direct effect on the rate of solidification in this initial stage, directly controlling the rate only after exhaustion of the undercooling that drives the initial stage. However it evidently affects the magnitude of this undercooling which is responsible for the initial stage, so will in that way influence it indirectly. Such models assume constant heat transfer coefficient during flight, which is not valid when convective cooling by the atomizing fluid is important. Recent measurements [22] for fluid atomization show that droplet velocity achieves a maximum some distance from the point of atomization (Fig. 4), while the fluid velocity decreases monotically with distance. Since convective heat transfer coefficient is a function of the difference between these two velocities, it is expected to vary with flight distance. This is a further complication in any complete analysis of this problem.

Heat and momentum transfer analyses have also been applied to the process of formation and cooling in the piston-and-anvil and twin-roll methods as well as to the melt-spinning and melt-extraction processes. Measurements [26] show that sample thickness tends to decrease with

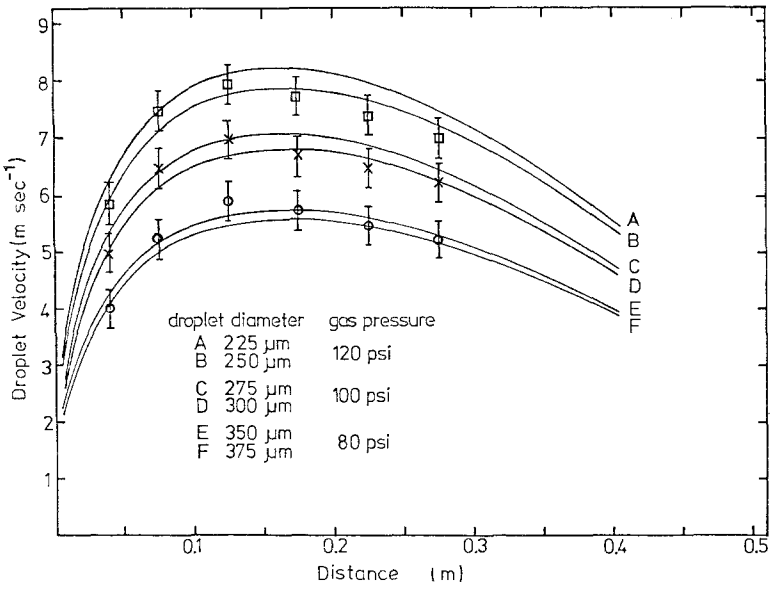

Figure 4 Mean droplet velocity as a function of flight distance and atomizing gas pressure for Al–2 wt % Cr [13].

increased superheat and especially with increased impact velocity in hammer-and-anvil quenching. This latter effect is in accord with a two-dimensional fluid flow/heat transfer model [27] in which final thickness is assumed to be determined by meeting of the two solidification fronts at the centre of radius and mid-thickness of the splat. Measurements [28, 29] for the twin-roll process show that sample thickness exceeds by a decreasing amount that of the initial roll gap as this is increased at least for sufficient feed rates. Measurements [29] of roll separating force decreasing with increasing ratio of rotational speed to melt feed rate are in good agreement with predictions from a fluid and heat flow model [30]. Non-uniformities of thickness across the width of metallic glass ribbon 60 mm wide made by this method were considered to arise from formability differences in the melt due to its higher temperature at points of jet impingement than elsewhere for the multi-jet melt feed arrangement employed [31]. In one attempt to improve control of product dimensions and cooling by twin-roll processing, a steel belt was run in contact with the rolls and through the roll gap along with the melt, in order to retain thermal contact with one roll and the belt for some distance beyond the nip of the rolls [31]. The unextended length of the thermal contact zone is somewhat longer in the CBMS and melt-extraction processes. The decrease of sample section dimension with increasing disc rotational speed for melt-extraction of Ni–20 wt % Cr alloy, at levels of thickness greater than the thickness solidified predicted on the basis of an assumed upper limiting heat transfer coefficient of $8\,kW\,m^{-2}\,K^{-1}$, led to the suggestion that fluid flow determined the product thickness [32]. A different study [33] in contrast reported thickness of melt-extracted Fe–20 at % B decreasing with increasing rotational speed (Fig. 5) at thickness levels close to those expected if solidification determined the thickness according to kinetics $z = qt^{1/2}$, where t is contact time and $q \sim 3\,mm\,sec^{-1/2}$ determined for large-scale solidification of steel in an ingot mould or in the water-cooled mould and secondary cooling zone of a continuous casting operation [34]. The relative importance of fluid flow and of

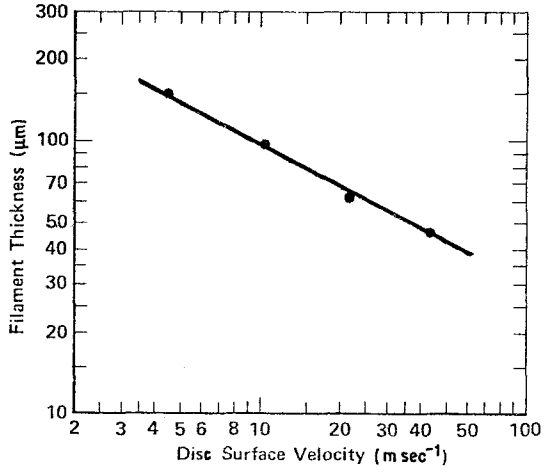

Figure 5 Thickness of pendant-drop melted-extracted Fe–20 at % B alloy fibre as a function of disc surface speed [33].

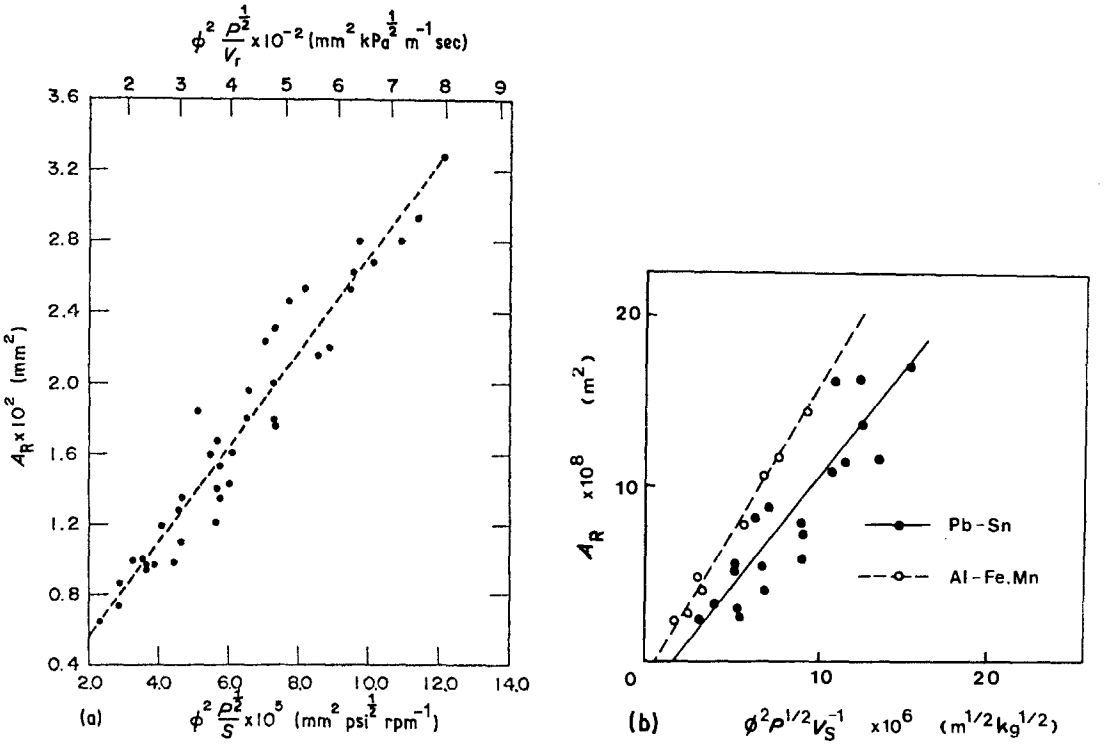

Figure 6 Ribbon cross-sectional area A_R as a function of $\phi^{1/2}p^{1/2}/\omega$ for melt-spun (a) metallic glass Fe–40 at % Ni–20 at % B [35] (published with kind permission of IEEE, © 1976), and (b) microcrystalline Sn–Pb and Al–(Fe, Mn) eutectic alloys [36].

solidification rate in determining thickness is an equally crucial consideration for CBMS and PFC processes. Measurements for CBMS of a metallic glass [35] and of two microcrystalline alloys [36] showed that ribbon cross-sectional area increased linearly with $\phi^2 P^{1/2}/\omega$ (Fig. 6) in accord with the Bernoulli and continuity equations where ϕ is melt orifice diameter, P is expulsion pressure and ω is chill-block rotational speed. Such and further measurements indicate ribbon thickness z and width w proportional to Q^n/v^m and Q^m/v^n respectively (Fig. 7), where Q is volumetric flow rate, v is

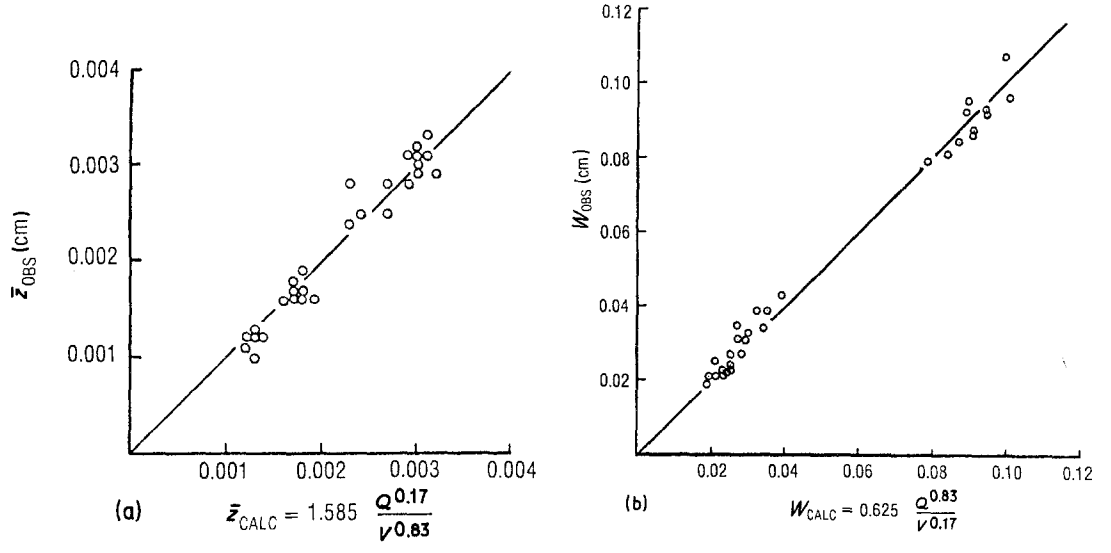

Figure 7 Observed against calculated values of (a) thickness $\bar{z}$ and (b) width w for melt-spun metallic glass ribbons of Fe–40 at % Ni–14 at % P–6 at % B alloy. Published with kind permission from the chapter Principles of Fabrication by Sheldon Kavesh in "Metallic Glasses" (American Society for Metals, Metals Park, Ohio, 1978) pp. 54, 55.

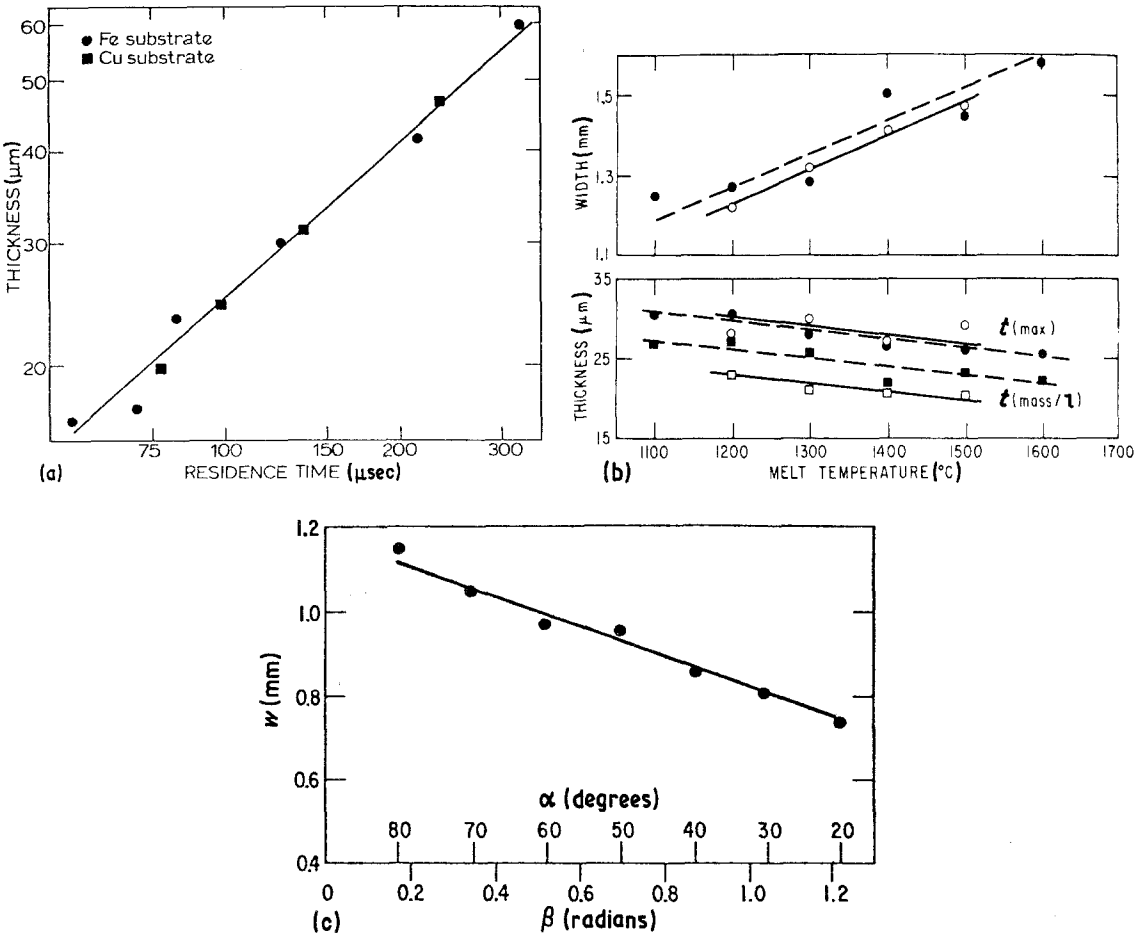

Figure 8 Thickness and/or width w of melt-spun metallic glass ribbon as a function of (a) residence time [42, 44], (b) temperature of melt [46] and (c) jet impingement angle β [39].

chill-block surface speed and n and m are typically ~ 0.2 and ~ 0.8 respectively [37–45]. Measurements (Fig. 8) also show that thickness $z \propto t^p$, where t is residence time defined as melt pool length l divided by v, and p is ~ 0.5 [38, 40, 41] or ~ 0.7 [42–45], that z is decreased and w is increased by increased melt superheat [46], and that w decreases with increasing jet impingement angle [39]. Kavesh [37] concluded that results then available for dependence of z and w on Q and v were not in perfect agreement with control by either thermal or momentum boundary layers, but values of n and m were nearer to his predictions for thermal than for momentum control. Both the details of formulation and the conclusions of Kavesh's model have been questioned, however [42–45, 47, 48], leading to remodelling in terms of momentum alone [42–45, 49] or involving combinations of thermal and momentum control [40, 50]. Good agreement with measured values of z as a function of v for metallic glass ribbon has been obtained (Fig. 9) both for momentum control alone [42–45] and its combination with thermal control [51]. Even for the most realistic and complete model however, final comparison between theory and experiment is inevitably subject to uncertainties as to the appropriate values to be used for key parameters such as kinematic viscosity as a function of melt supercooling, in the case of momentum modelling, and of heat transfer coefficient in the case of thermal modelling. Complete modelling of CBMS also needs to include prediction of melt pool length and width as a function of process conditions, since these evidently determine ribbon thickness and width respectively. PFC differs in that ribbon width in stable operation is constrained to be nearly equal to the width of the delivery slot so that ribbon thickness should be determined directly from the continuity equation $Q = A_0 u = wzv$ where A_0 and u are

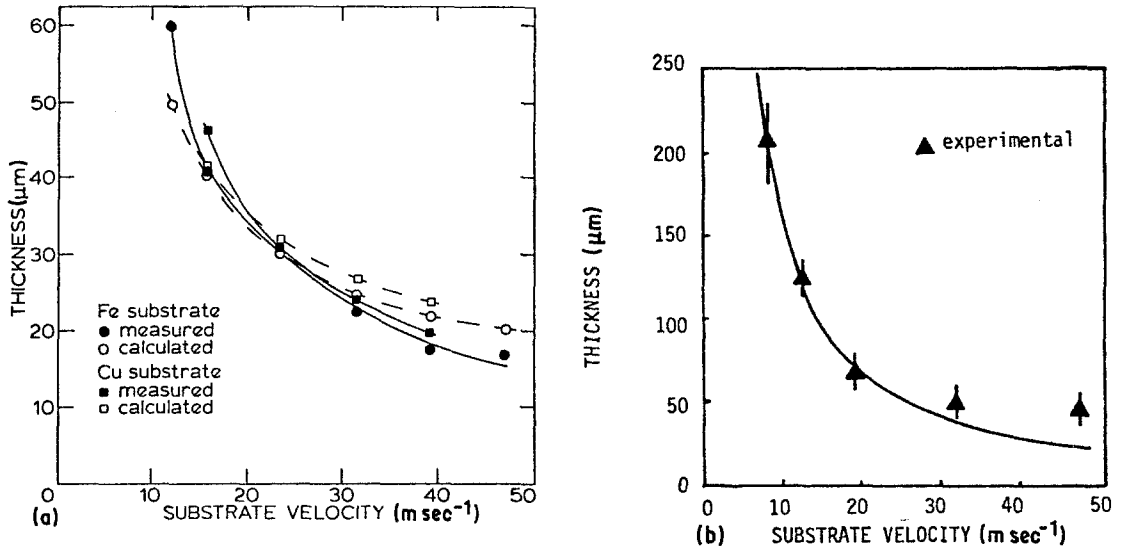

Figure 9 Observed and predicted thickness as a function of chill-block surface speed for melt-spun ribbon of (a) Fe–13 at % P–7 at % C metallic glass [42–45] and (b) microcrystalline Al–4.5 wt % Cu [51].

inside cross-sectional area and stream velocity at the exit of the delivery slot and $u = 2P/\rho$ according to the Bernoulli equation, where P and ρ are expulsion pressure and density of the issuing melt. Measurements [52] of z as a function of v and P lend some support to these predicted dependencies.

Modelling of directed-energy processing is simplified by the insignificant role of fluid flow in controlling product dimensions, quite unlike the situation in spray, piston-anvil, twin-roll or spinning methods, so that consideration of heat transfer alone forms the essential basis for modelling. Even this aspect is simplified by the expected perfect contact between melted zone and unmelted base material acting as the heat sink. A complication does arise when a laser is the energy source in that the fraction of incident energy actually absorbed (rather than reflected) can be small and undetermined except by implication. Both analytical [53–56] and numerical [57, 58] heat flow modelling has been carried out to predict depth melted, melting and solidification front velocities and temperature histories as a function of input variables, but few attempts have been made as yet to compare predictions with available experimental measurements. For depth melted, z, the good agreement between predictions and observations obtained for electron beam [57] and laser [59] traversing is for larger penetrations than would be characteristic of RSR-conditions. Excellent parametric and absolute agreement (Fig. 10) was retained [67, 68, 73] to depth melted as small as 60 μm for TIG and electron beam traversing of an austenitic stainless steel [55]. The corresponding predicted values were several times lower than those observed [58] for laser traversing of a superalloy, in this instance attributable to non-adsorption of a large proportion of the incident energy. Reasonable agreement has been claimed [69] when due allowance is made for this reflection of incident radiation from the sample surface. Indications [74, 75] from reflectivity measurements of the duration of melting of silicon in laser traversing show reasonable agreement with predictions [67, 68] along with estimates of the solidification front velocity. Similarly good agreement with predictions has been reported [76]

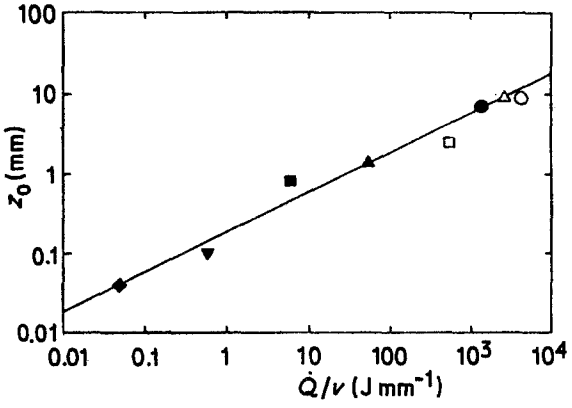

Figure 10 Depth melted z_0 as a function of heat input per unit length $\dot{Q}/v$ for TIG and electron beam traversing of type 310 stainless steel [55, 73].

for front velocities estimated by measuring time dependence of conductance of the molten layer, making use of the fact that resistivity drops by a factor of 30 when silicon melts.

3. Effects

The actual product of rapid solidification is sensitive both to alloy composition and to solidification conditions. Early attempts to represent this behaviour [77] involved mapping fields of occurrence of different products as a function of composition and cooling rate (Fig. 11a). While composition can be determined with some confidence, cooling rate on such plots was normally estimated from thickness z or dendrite arm spacing, and is thus subject to uncertainty. The general practice is to map constitution as a function of composition alone [78] for just one condition of quenching from the melt (Fig. 11b), yielding compositional limits for formation of various products for the particular set of processing conditions involved. Generalization of such results into two-parameter plots, for example based on the periodic table [79], or as heat of mixing or solution against atomic size ratio [80] or as liquidus departure from ideality against compostional factor [81] are all means of identifying compositions likely to be susceptible to a particular effect under given formation conditions. Much less attention (Fig. 12, taken from [82], shows one exception) has been given to the experimental determination of critical cooling rates (or thickness) for formation of particular products of specified composition, for comparison with predictions from kinetic theory. Cooling in this context is simply an indirect means of achieving the supercooling or solidification front velocity required to achieve the desired effect. Achievement of such effects at lower cooling rates provides more scope for *directly* controlling either (a) the level of undercooling (i.e., temperature) at which solidification occurs via controlled cooling and nucleation of small droplets [83], or (b) the solidification front velocity via steady withdrawal of a sufficiently thin sample through a high temperature gradient. This latter technique has been applied [84] to indicate the conditions for suppression of primary equilibrium Al_3Fe and of the Al–Al_3Fe eutectic in hypereutectic aluminium–iron alloys in favour of Al–Al_6Fe eutectic with or without αAl dendrites, where Al_6Fe is considered to be a non-equilibrium phase (Fig. 13). Further complications arise from the subsequent identification [85, 86] of at least one other non-equilibrium phase, Al_mFe or Al_xFe, and the progressive elimination of interdendritic eutectic with further increase in front velocity in favour of monolithic interdendritic crystalline or ultimately non-crystalline phases [87–89]. This occurs together with progressive extension of solid solubility of Fe in αAl, eventually resulting in partitionless solidification to form featureless single-phase αAl solid solution with the same composition as the parent melt [90]. The same technique has been applied [91] to alloys of the palladium–silicon–copper system known to be especially susceptible to glass formation at compositions near 17 at % Si and 6 at % Cu. The effect of progressively changing this copper : silicon ratio from 21 : 1 through 17 : 6 to 12 : 12 is shown in Fig. 14. Here glass formation is effectively replacing eutectic growth at growth velocities exceeding 2.5 mm sec^{-1}, and like the eutectic, can evidently form in the presence of crystalline κ-phase in sufficiently hypereutectic alloys. The boundaries between fields, as shown in Fig. 13, are readily predicted by applying the principles of competitive growth, provided that growth temperature of the competing solidification modes can be reliably predicted as a function of growth velocity and composition, and that effects of nucleation are negligible. Nucleation effects evidently cannot be neglected in the corresponding situation for iron–carbon alloys, in which difficulty of nucleation of austenite-cementite (white iron) eutectic results in persistence of austenite-graphite (grey iron) eutectic to higher growth velocities than predicted by competitive growth considerations alone [92].

The contributions to crystal formation of both nucleation and growth have been taken into account in kinetic models [93–96] that predict critical cooling rates for glass formation in reasonable agreement with experience for the main categories of glass-forming solid. Corresponding nucleation-and-growth analyses for competition between alternative *crystalline* phases and morphologies at high solidification rates have yet to be developed. Complications arise from the difficulty of realistically specifying the nucleation and growth kinetics of so many possible alternatives, when quite small differences can evidently determine the final outcome. A starting point would be to predict the kinetic conditions for partitionless formation of single-phase extended

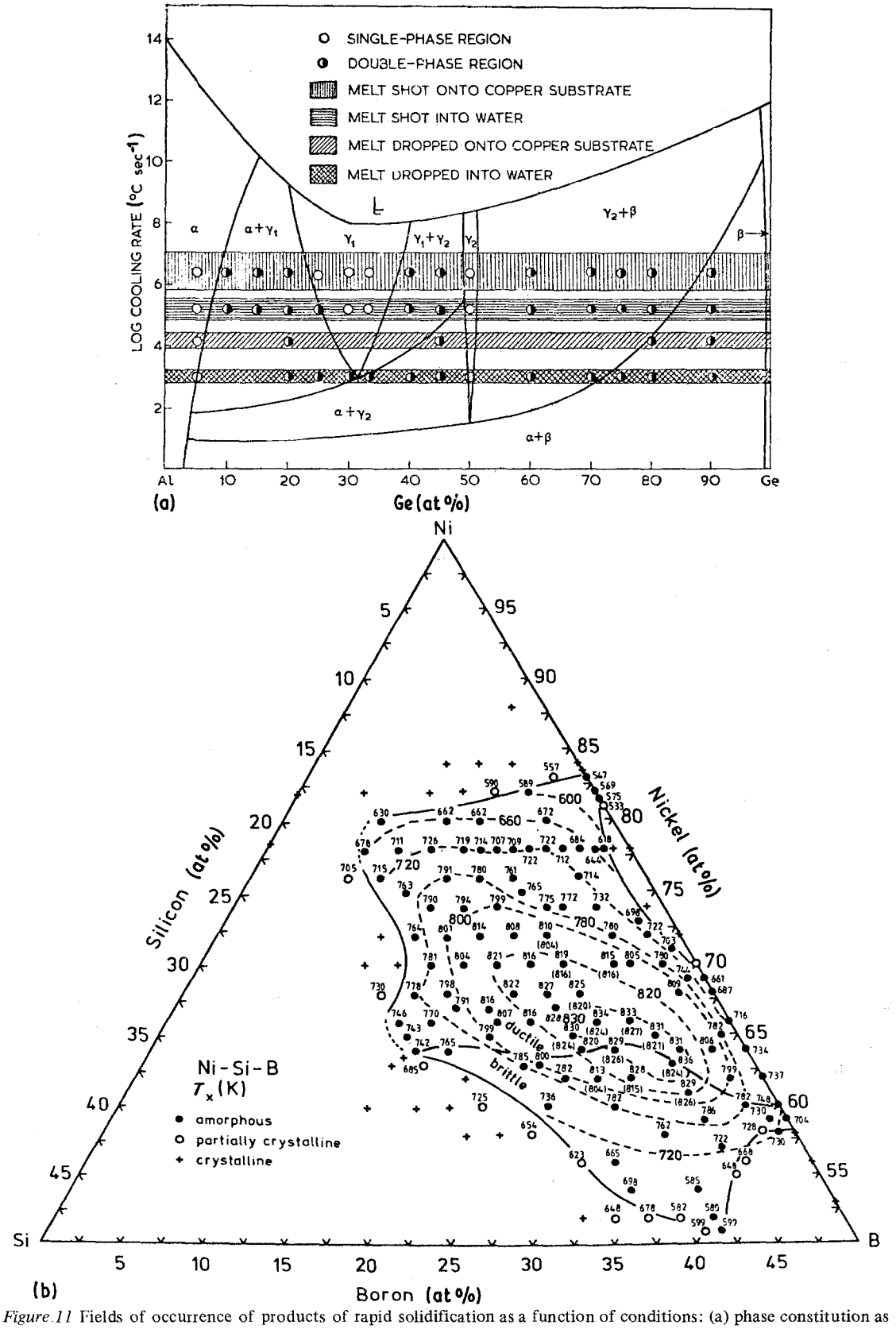

Figure 11 Fields of occurrence of products of rapid solidification as a function of conditions: (a) phase constitution as a function of alloy composition and cooling rate in Al–Ge [77]; (b) ternary composition field glass formation in Ni–Si–B melt-spun ribbon of thickness 17 ± 3 μm [78].

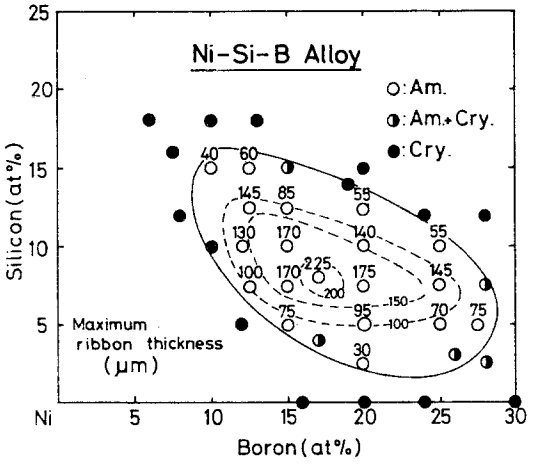

Figure 12 Critical thickness for glass formation as a function of composition for melt-spun ribbons of Ni–Si–B alloys [82].

solid solution based on the terminal phase α of an alloy system. Progress is being made on both the thermodynamic and growth aspects of this problem. A minimum thermodynamic condition is that the alloy must be cooled below its T_0 temperature (at which the free energies of liquid and solid α of this composition are equal), without formation of any other phase. For a hypereutectic alloy this involves suppression of formation of primary equilibrium β-phase, of primary or secondary (intercellular or interdendritic) α–β eutectic, and of any alternatives involving non-equilibrium phases (including glasses). Certain alloy systems between components with the same crystal structure, such as silver–copper (Fig. 15), can have T_0 against composition curves that are continuous between the components even if they show restricted solid solubility and eutectic formation at equilibrium. Undercooling below T_0 then allows the *possibility* of continuous solid solubility under conditions of sufficiently rapid solidification. Undercooling to below the extended solidus temperature of a phase is considered to satisfy conditions *fully* for partitionless formation of that phase from the melt [98, 99]. Even if the T_0 curve is continuous, the extended solidus curve need not be, as shown for the silver–copper system in Fig. 15, giving a retrograde solidus requiring *solute trapping* [100–108] at the solidification front to account for solid solubility extension above 15 at% copper in silver and above 5 at% silver in copper (the maximum, C_{MAX}, of each retrograde solidus). The basis of solute trapping is that, while solvent atoms can transfer from liquid to solid by making only small shifts in

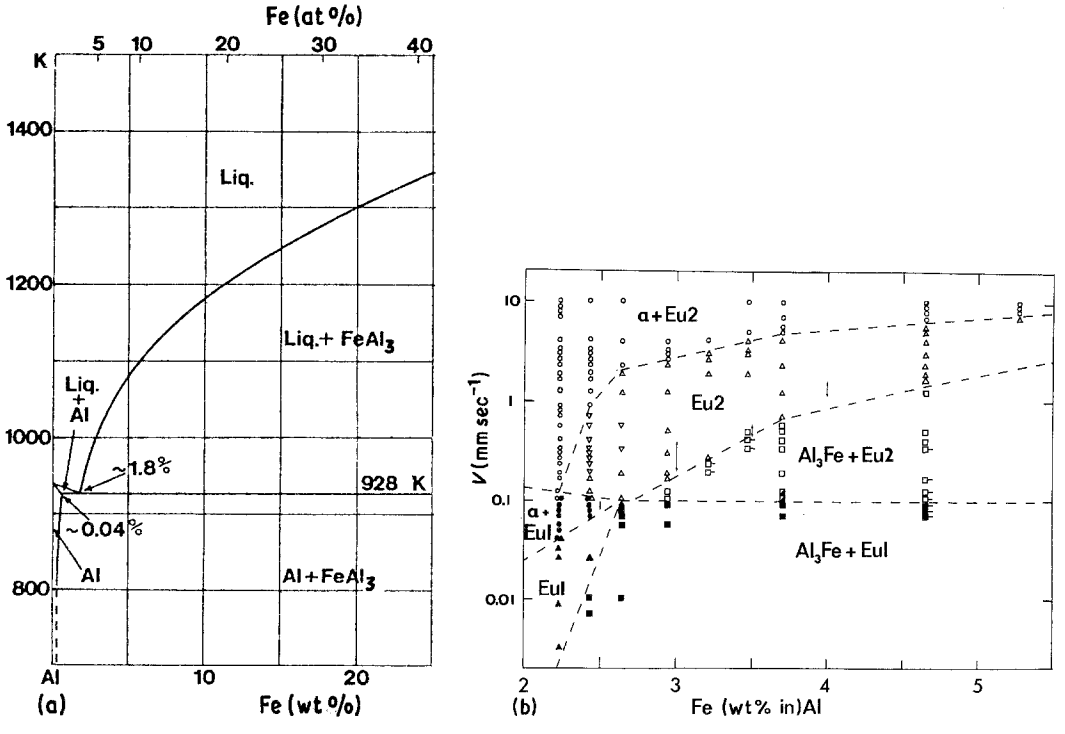

Figure 13 Dependence on alloy concentration for Al–Fe alloys of (a) equilibrium constitution and (b) product morphology and constitution as a function of growth velocity v [84].

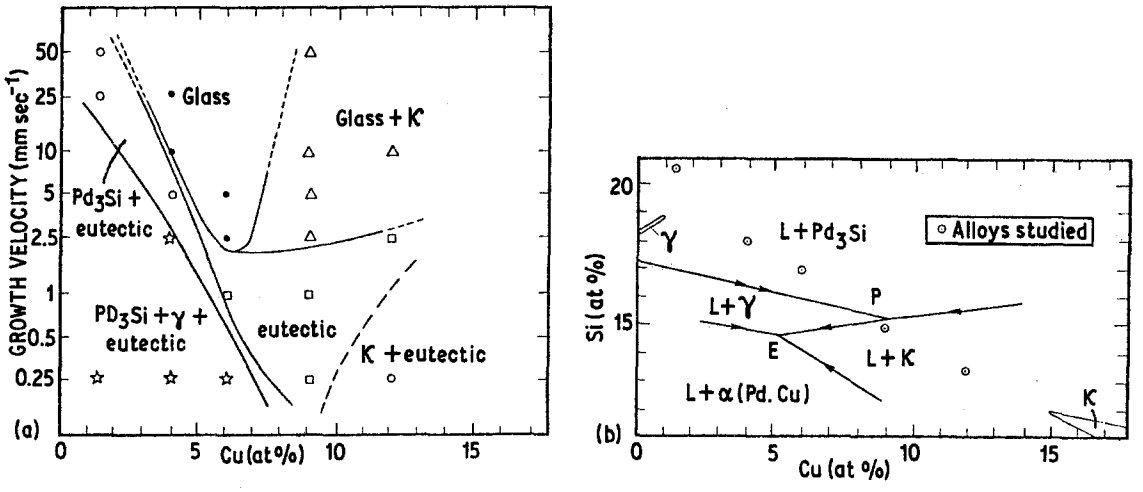

Figure 14 Dependence on alloy concentration of (a) product morphology and constitution as a function of growth velocity and (b) equilibrium liquidus surfaces, for Pd–Cu–Si alloys [91].

position and bonding, solute atoms would need to diffuse long distances to avoid being engulfed by a rapidly moving solidification front. For systems (e.g. Fig. 16, [109]) also showing T_0 curves that are not continuous, the intervening composition range will be forbidden to partitionless solidification based on either of the terminal phases, making such systems especially vulnerable to formation of a non-equilibrium crystalline phase or a glass in this composition range. It has been suggested [109] that C_{MAX}/k_0 should give a reasonable indication of this T_0 limit to solute trapping under such circumstances, where k_0 is the "equilibrium" partition coefficient corresponding to C_{MAX}. Table I shows that observed maximum values C_{EX} of extended solubility of several solutes in silicon and of cadmium in zinc are, with one exception, intermediate between C_{MAX} and C_{MAX}/k_0, consistent with solute trapping within its upper limit C_{MAX}/k_0 (though the corollary that such limits to solute trapping in the terminal phases should, as a result, also bound an intervening composition range for glass formation [97] has yet to be demonstrated for rapid solidification from the melt). The extent of departure from equilibrium at the solidification front associated with solute trapping is indicated [110] by observed partition coefficients k in the range $0.15 < k < 1$ for the solutes in silicon in Table I at estimated solidification front velocities

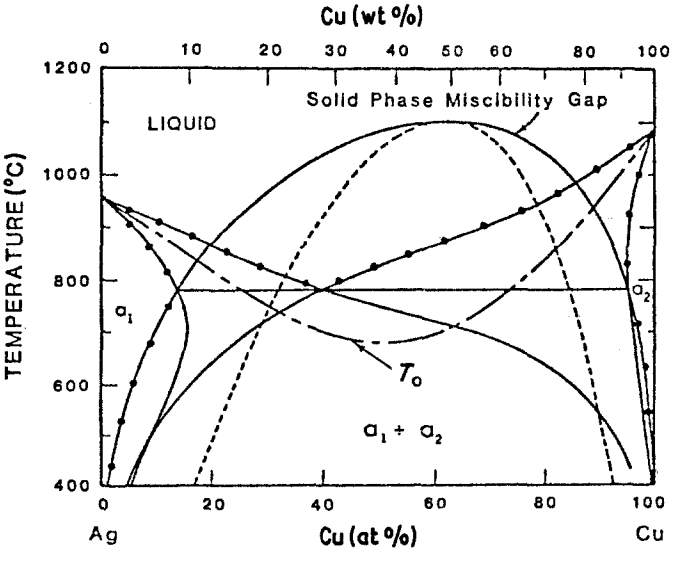

Figure 15 Dependence on alloy concentration of boundaries of equilibrium and extended phase fields for Ag–Cu alloys, showing a continuous T_0-curve but retrograde solid solubility curves [97].

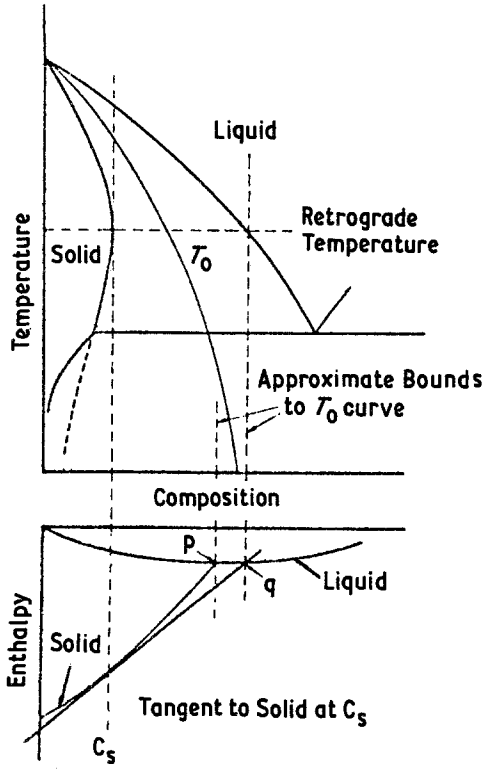

Figure 16 As Fig. 15 but for a system showing a discontinuous curve T_0-curve as well as retrograde solid solubility [109]. Note that the figure approximates the solid enthalpy curve by a straight line (drawn to point q). The accuracy of the estimated bound to the T_0-curve is therefore best when Henry's Law is obeyed as for nearly ideal solutions. Thus, apparent failures of the approximations occur (e.g. with Ag–Cu, Fig. 15) where both solid phases exhibit metastable retrogrades with no bound on the T_0-curve (private communication from J. W. Cahn, April 1983).

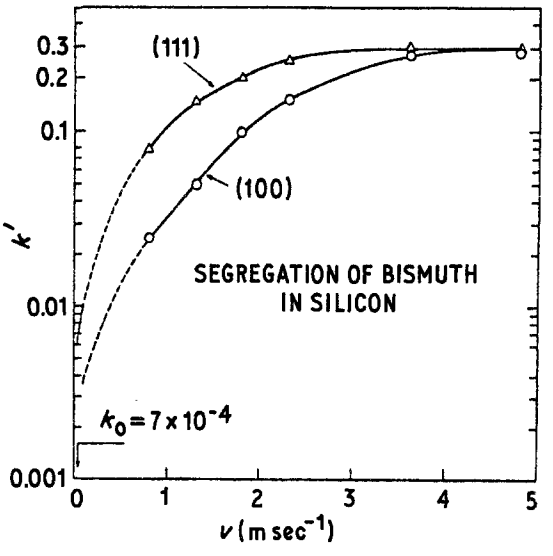

Figure 17 Dependence of non-equilibrium partition coefficient k' on solidification front velocity v for bismuth in (1 0 0) and (1 1 1) silicon [107].

of 2.7 or 4.5 m sec^{-1} produced by laser-directed energy processing. Such values of k compare with equilibrium values (k_0) as low as 0.0004 for indium in silicon and are in reasonable accord [104] with predictions by atomic kinetic modelling [102–104, 108] of the underlying velocity-dependence of k, increasing from k_0 to unity over a characteristic range of increasing velocity. Fig. 17 shows some actual results [107] on the velocity-dependence of k for bismuth in silicon from laser-directed energy processing experiments in which the variation in front velocity v over the range 1 to 5 m sec^{-1} was achieved by changing the combination of silicon substrate temperature and laser pulse characteristics and using heat flow modelling to compute the resulting values of v. It is notable that depths melted $z < 0.1\,\mu$m have been achieved by using picosecond [111, 112] or nanosecond [65, 66, 113] laser pulse lengths giving estimated front velocities as high as 20 m sec^{-1} [114, 115] resulting for the first time in production of amorphous silicon by rapid solidification from the melt. This ability to generate and control high solidification front velocities > 1 m sec^{-1} has enabled predictions concerning interface stability at high v to be tested, again for the first time. Instability is predicted [116] when the (destabilizing) constitutional supercooling parameter

TABLE I Estimate C_{MAX}/k_0 (10^{20} atoms cm^{-3}) of maximum attainable extension of solid solubility by solute trapping, compared with results C_{EX} obtained by rapid solidification for five solutes in silicon and for cadmium in zinc [109].

Solute	Cd*	Ga	In	As	Sb	Bi
C_{MAX}	0.025*	0.45	0.008	15	0.7	0.008
k_0	0.11*	0.008	0.0004	0.30	0.023	0.0007
C_{MAX}/k_0	0.22*	60	20	50	30	10
C_{EX}	0.10*	4.5	1.5	60	13	4

*In Zn, with concentrations in mol. fractions

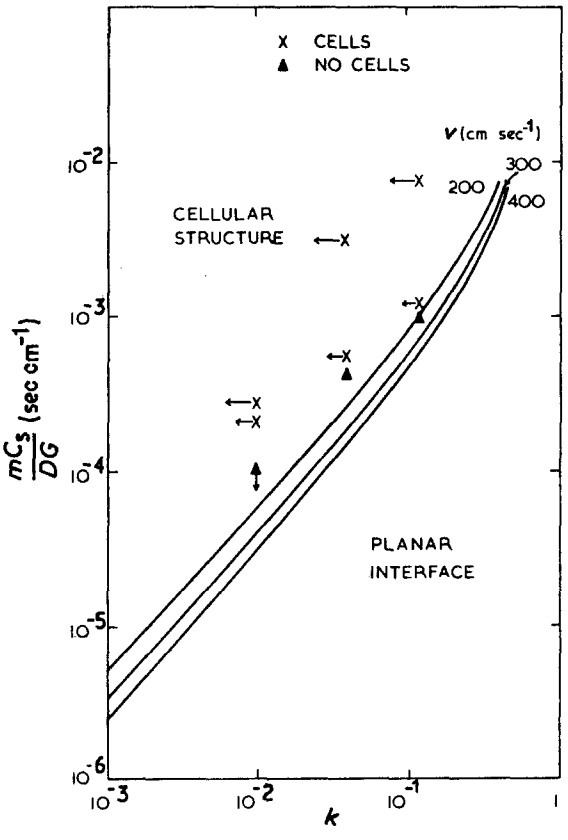

Figure 18 Prediction compared with observation for the condition giving a planar to cellular transition for laser-directed energy processing of indium in silicon [117].

$[m_L C_s(1-k)/kG](v/D)$* (which is the ratio to *actual* thermal gradient G at the interface of corresponding *liquidus* gradient $m_L G_c$ there resulting from actual concentration gradient G_c in the melt, where m_L is liquidus slope from the phase diagram, C_s is solute concentration in the solid, and D is solute diffusion coefficient in the melt) exceeds a critical value. This value is a complex function of k and the (stabilizing) capillarity parameter $(k\Gamma/G)(v/D)^2$ (which embodies the ratio to G of the Gibbs–Thomson capillary coefficient $\Gamma = \gamma/\Delta S$ where γ is interfacial energy and ΔS is entropy of melting). Here G is the weighted value for the solid and liquid phases at the solidification front. Fig. 18 compares the predictions of instability theory with actual results for indium in silicon on a plot of concentration parameter $m_L C_s/DG$ as a function of k, and shows that breakdown from planar (stable) to cellular (unstable) growth occurs at values of $m_L C_s/DG$ typically within a factor of 2 of those predicted, and that the predicted trend of critical $m_L C_s/DG$ increasing with increasing k is in good accord with experiment [117]. Predictions of velocity-dependent cell size at the limit of instability are also found to be in good agreement with theoretical predictions [118, 119]. The velocity required to produce interface stability with 0.1 to 1 wt% silver or manganese in aluminium were found to be several times larger than predicted [120], possibly attributable to uncertainties in the values of D and Γ for aluminium–manganese alloys. Such comparisons are further complicated in the case of results from spray or chill methods by uncertainties concerning the magnitude of heat transfer coefficient and undercooling applicable, and their effects on interface velocity and stability as affected by any recalescence that occurs [23, 24, 96, 121–124]. The observation of an initial partitionless, featureless, predendritic first stage of solidification associated with rapid motion of the solidification front into initially undercooled melt, followed a cellular or dendritic second stage accompanied by partitioning, segregation and second phase, and associated with a lower solidification front velocity limited by external heat extraction, is widespread [88, 90, 98, 124–126] and significant. The ability to predict correctly the extent of the featureless zone as a function of experimental variables would be a major step forward in modelling such microstructural effects. The practical importance of maximizing the proportion of partitionless solidification in a particular sample should also not be underestimated.

Practical importance is also attached to the scale of microstructure produced by partitional cellular and dendritic solidification. Much use has been made of power relationships (Fig. 19) between dendrite spacing λ or eutectic spacing Λ and cooling rate ϵ or solidification front velocity v for estimating locally operative ϵ and v from measured λ or Λ. The dendrite relationship $\lambda = B\epsilon^{-n}$ has some theoretical basis when secondary dendrite arm coarsening controls the final spacing, giving $n = 1/3$ and, for an alloy such as Al–4.5 wt% Cu, $B \simeq 50\,\mu m\ K^{1/3}\ sec^{-1/3}$. While this is reasonably consistent with experimental data for appropriate aluminium–copper and aluminium–silicon alloys, wide variations in exponent n and proportionality factor B are found in practice (Table II), attribu-

*This simplifies to $(k\Delta T_0/G)(v/D)$ when equilibrium partitioning occurs at the interface where ΔT_0 is temperature interval between liquidus and solidus.

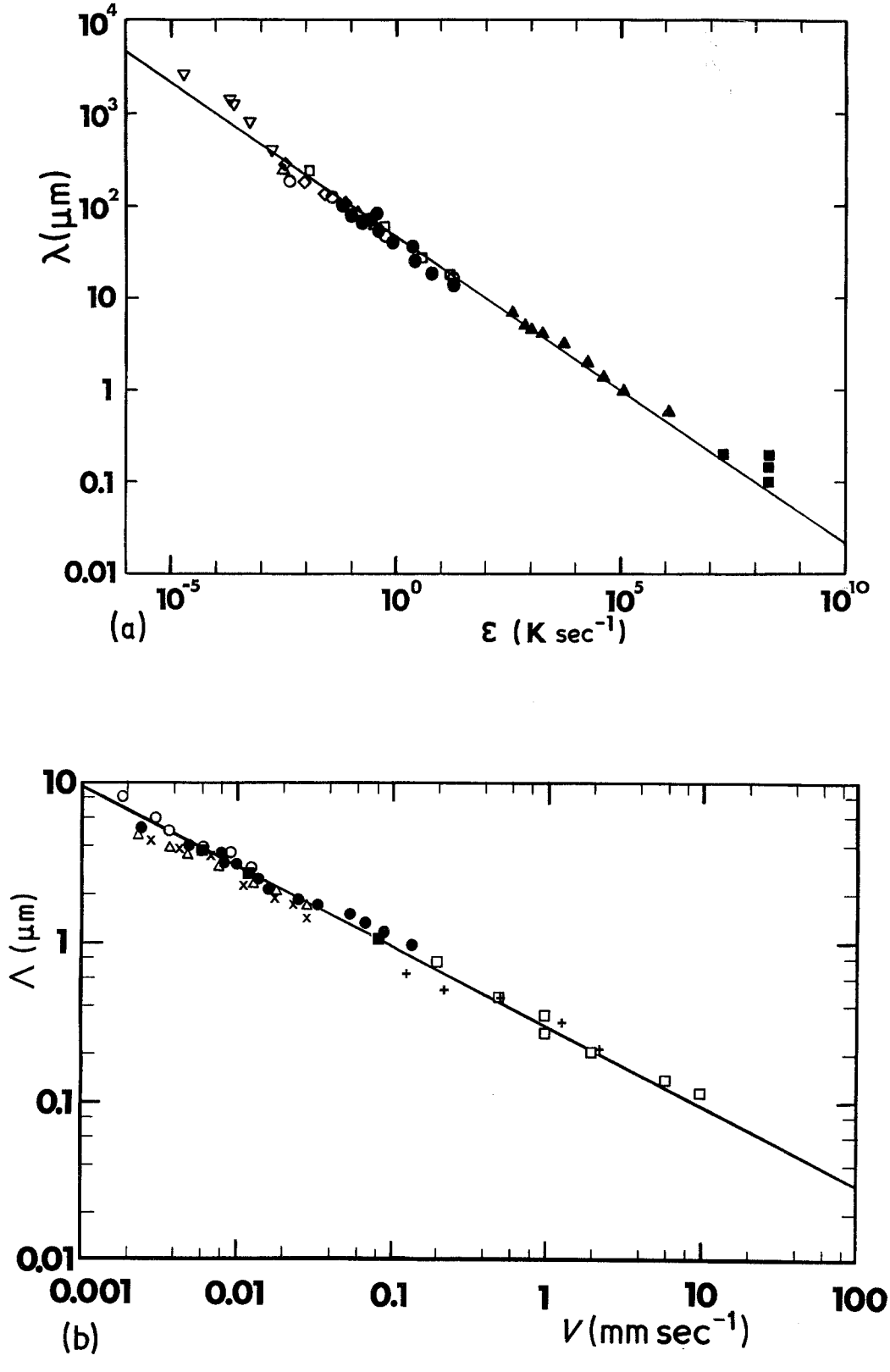

Figure 19 (a) Dendrite cell size λ as a function of creep rate ϵ for Al–4 to 5 wt % Cu (open points) and Al–7 to 11 wt % Si (filled points) [5]. (b) Eutectic interlamellar spacing Λ as a function of growth velocity v for Al–Al_2Cu eutectic [5].

TABLE II Observed dependence of dendrite spacing λ on cooling rate ϵ according to the power relation $\lambda = B\epsilon^{-n}$ [73].

Alloy composition (wt %)	Range of cooling rate (K sec^{-1})	Exponent n	Parameter B ($\mu m\ K^n\ sec^{-n}$)	Reference
Sn – 15 Pb	0.005 to 50	0.49**	60**	[292]
Al – 5 to 40 Cu	0.01 to 30	0.25	18 to 45	[293]
Al – 4.4 to 4.6 Cu	2×10^{-5} to 300	0.39	41	[294]
Al – 10.5 Si	400 to 1.2×10^5 †	0.33	47	[295]
Al – 7 Si–0.3 Mg	~ 0.01 to 20†	0.34◇	42◇	[131]
Cu – 0.2 to 0.8 Zr	1 to 10^7	0.40	160	[296]
Ni – 27 Mo	0.1 to 10	0.55	44	[292]
Ni – 19 Cr–3 Mo–0.8 Ti (Inconel 718)	0.1 to 100	0.40** 0.34	141** 34	[292]
Ni – 20 Cr–13.5 Co–4.3 Mo – 2.9 Ti–1.2 Al (Waspaloy)	0.05 to 20	0.29**	112**	[292]
Co – 25 Cr–10 Ni–7.5 W (X-40)	0.1 to 200	0.32** 0.27	90** 40	[292]
Fe – 20 Mn	60 to 6×10^6 ‡ 60 to 1400‡	0.40** 0.25	20** 150	[55]
Fe – 25 Ni	0.0012 to 1.7×10^6 †	0.32	60	[297]
Fe – 18 Cr–1 C (440 stainless steel)	15 to 10^5†	0.41	60	[297]
Fe – 0.03 Si–0.02 O	15 to 1500†	0.50*	4*	[297]
Fe – 18 Ni–9 Co–5 Mo–0.9 Ti (Maraging 300 steel)	0.1 to 1400	0.30	40	[298]
Ti – 2 to 30 Al, Fe, Ge, Mo or V	0.2 to ~ 150†	0.31 to 0.53◆	16 to 124◆	[299]

†Measured cooling rates
‡Cooling rates calculated from heat flow theory.
All other data are for secondary arm spacing
*Silica inclusion size
**Primary spacing
◆function of alloy composition
◇Dendrite cell size

table to approximations made in the coarsening model, contributions from primary spacing predicted [127, 128] to have a more complex dependence on front velocity v and temperature gradient G, and increasing suppression of secondary arms at high cooling rate to stabilize a cellular structure. The theoretically-based relation for eutectic growth, $\Lambda = Bv^{-n}$ with $n = 1/2$ and $B \sim 10\,\mu m^{3/2}\,s^{-1/2}$, is again reasonably consistent with experiment for several eutectics, but spacings can be variable up to ten times predicted optimum values for irregular eutectics such as aluminium–silicon and iron–carbon [129], and the exponent n can in practice depart from the ideal predicted value of 1/2. The outcome of predictions [130] of the dependence of grain size on cooling rate is especially sensitive to values chosen for physical parameters governing rates of nucleation and growth, and there is an almost total absence of experimental data on dependence of grain size on cooling rate during solidification that could be compared with predictions. Systematic studies of the effect of magnitude of cooling rate during solidification on *properties* are also rather few, but nevertheless significant. Classic work established the effect of increased cooling rate in increasing tensile strength and ductility of casting alloys through its effect in reducing dendrite spacing [131]. Its effects in multiplying strength through dispersion hardening [88, 132] and in increasing fatigue and stress rupture lives through refinement of metallic impurity inclusions [133] have been demonstrated. Such comparisons are essential if the precise contribution of rapid solidification to observed property changes is to be assessed in given circumstances.

The properties actually resulting from rapid solidification evidently depend on the structural changes produced in each particular case. For example, metallic glasses are characterized by high mechanical strength with ductile behaviour in bending, shear and compression; high reactivity or high corrosion resistance depending on composition; superconductivity or high resistivity depending on temperature; and outstanding soft magnetic behaviour for appropriate compositions [5]. High mechanical strength is evidently also attainable in microcrystalline materials as a result of refined microstructure combined with increased alloying [134] and this combination can at the same time give rise to superplastic behaviour at elevated temperatures [135]. Improvements in such properties as thermal stability and elastic stiffness can result from being able to make alloy additions prohibited to ingot processing [136]. The minimum capability of achieving more consistent properties through consolidated sections independent of their size is itself a notable effect of rapid solidification compared to ingot solidification, leading to more predictable and controllable behaviour in processing and in service.

4. Applications

Although academic curiosity evidently motivated Duwez's discoveries [3, 4] of two decades ago that formed the nucleus of current activity in rapid solidification, the principles of much of present-day RSR-processing were established by the turn of the century entirely with industrial applications in mind. The invention of metal atomization is usually attributed to Marriott [137] who in 1872 patented a method for producing lead powder, for conversion to oxide or salts, by drawing-off and spraying molten lead by means of a steam injector*. A process for making non-adherent splats by rotary spraying on to surrounding baffles was patented in 1906 [138]. Spray-deposition of atomized metal droplets to form a continuous adherent deposit has been in use for most of the century, both to repair damaged or worn machine parts and to impart corrosion or wear resistance required in service. Melt-extrusion through an orifice to make soldering wire was patented in 1882 [139], while chill-block melt-spinning was patented in 1908 [14] followed in 1909 by a process resembling melt-drag [140]. Development of directed-energy-processing has occurred as part of the search for possible applications of power lasers and electron beams.

Concentration by the scientific community during the 1960s on further exploring the constitutional effects identified by Duwez did not entirely exclude some attention to applications. These included an inductance thermometer [141] based on the several-fold increase in magnetic moment of an RSR-processed iron–cobalt–vanadium alloy with decrease of temperature to 14 K, use of splat-cooled specimens as homogeneous standards for electron probe [142] and neutron activation analysis [143] and to monitor

*For a history of the related shotting process, dating from c. 1650, see W. Johnson, A. G. Mamalis and H. Hunt, *Metall. Met. Forming* 43 (6) (1976) 68.

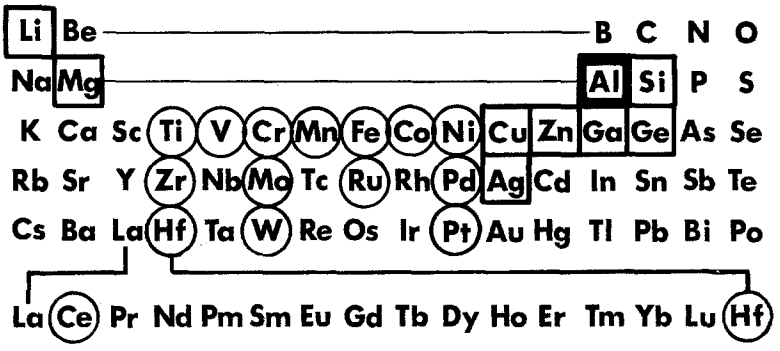

Figure 20 Effect of RSR processing on extent of solid solubility in aluminium: □ equilibrium solid solubility > 1 at %; ○ solid solubility extended to > 1 at % by RSR-processing.

atmospheric pollution by sulphur dioxide [144]. Some attention was also given to potential nuclear [145, 146] and automotive [148] applications of RSR-processing. The main stimuli to develop applications in the 1970s and to date have been the pioneer efforts of Allied in the USA to establish applications for metallic glasses, as a new class of material, of such as Crucible in the USA and ASEA in Sweden to develop hot-isostatic-pressing of pre-alloyed powder as high-yield routes to near-net-shape aerospace and tool parts, and by United Technologies to develop directed-energy and rotary-atomization processing as routes for aerospace materials development.

No attempt will be made to review fully all of the developments that have taken place or are in prospect. That task is the subject of a current proposal by Battelle Columbus Laboratories [149]. Instead, a broad overview will be presented under five main headings: high-strength structural materials; tool and bearing materials; high-temperature materials; corrosion-resistant, catalytic and storage materials; and, finally, electrical and magnetic materials.

4.1. High-strength structural materials

The beginning of the application of RSR-processing to develop structural materials can be traced back at least 30 years to a report by Busk and Leontis [150] of improved combinations of properties in a magnesium alloy consolidated by extrusion from pre-alloyed atomized powder. Non-transition engineering metals such as magnesium, aluminium, zinc, tin and lead are prime candidates for alloy development using RSR-processing in that their positions in the periodic table impose restrictions on the equilibrium solid solubility of all but a few adjacent elements. Aluminium is an extreme example in being limited (Fig. 20) to only eight or nine alloying elements (lithium, magnesium, silicon, copper, zinc, galenium, germanium, silver and, possibly, mercury) that show solid solubilities exceeding one atomic per cent. As a result, development of aluminium alloys by wrought-ingot processing has been confined until recently to essentially four of these additions, that is, magnesium, silicon, copper and zinc. This contrasts with the situation for alloying of titanium, iron, cobalt, nickel, copper and silver for which as many as 49, 29, 29, 31, 21 and 18 alloying elements respectively are solid-soluble at equilibrium to more than one atomic per cent. Conventional wrought aluminium alloys consequently show limitations, especially in strength, elastic modulus, thermal stability and stress-corrosion resistance, in spite of their formability and low density. Development of powder metallurgy (P/M) aluminium alloys through consolidation of atomized pre-alloyed powder was started by Alcoa and Kaiser in the USA in the 1950s. The initial programmes [151–153] included increasing the levels of conventional wrought alloy additions (magnesium, silicon, copper, zinc) and, in parallel, exploration of compositions based on large additions of transition metals such as chromium, manganese, iron, cobalt and nickel, normally limited to low levels in conventional alloying, but which markedly improve modulus and thermal stability. Yield strengths as high as 850 MPa were achieved [154] after heat treatment of such extended aluminium–zinc–magnesium–copper compositions, considerably higher than obtainable in conventional high strength alloys, such as 7001 and 7075, wrought from ingot. Continuing programmes have developed compositions showing no evidence of pit blistering or exfoliation for strength levels ~ 700 MPa at which wrought ingot 7001 shows extensive exfoliation. These compositions also showed stress corrosion and fatigue resistance superior to wrought-ingot 7075 [155, 156].

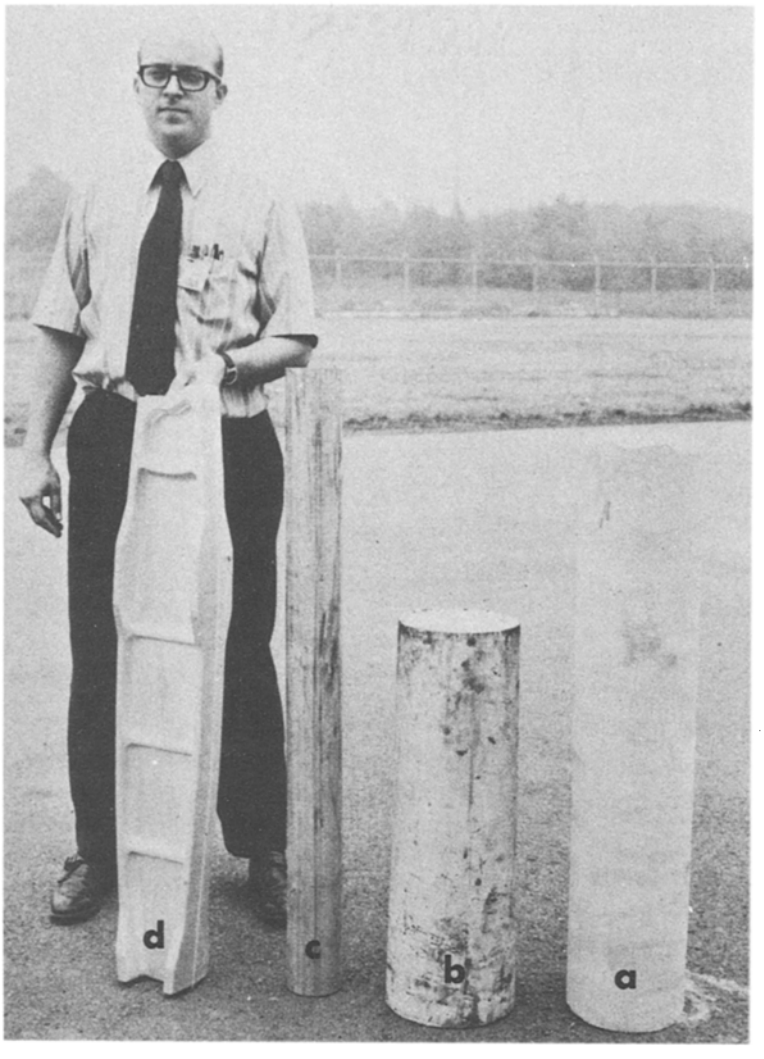

Figure 21 A production sequence for an aircraft forging made from atomized pre-alloyed powder. (a) Cold compact; (b) hot-pressed compact; (c) extruded rod; (d) forging [155].

Forgings of near-net shape parts for aircraft structural applications (e.g. Fig. 21) have been made for evaluation from hot-pressed billets of promising compositions up to 1500 kg in size. Two such first-generation alloys 7090 and 7091 contain a small addition of cobalt to control grain size and offer a superior balance of properties to conventional 7xxx wrought ingot alloys. Boeing are reported [157] to have specified 7090 for a 50 kg forged landing gear door actuator for their 757 airliner, so making the first step into the market place for this new generation of materials.

Improvements in elastic stiffness of aluminium alloys without loss of other properties are of particular interest to airframe designers, especially if combined with reduced density. Alcoa identified as long ago as 1958 the increase of elastic modulus occurring in atomized powder alloy extrusions with increasing volume fraction of transition metal aluminide, dispersed by atomization through the aluminium matrix [152, 153]. Thus, Young's modulus can exceed 100 GPa, albeit with some increase in density, for Al–16 wt % Mn [158], compared with ~ 70 GPa for pure aluminium and conventional wrought alloys. Additions of lithium have the special attraction of reducing density (by 3% per wt % Li) as well as increasing modulus (by 6% per wt % Li) [159], and so are currently under intensive investigation by both the wrought ingot and rapid solidification routes. RSR-processing has the advantages of refining both matrix grain size and intermetallic dispersoid particle size, which should minimize the slip localization shown to be a prime cause of inadequate ductility and fracture

toughness in high-strength wrought ingot alloys containing lithium. A current programme has already shown that RSR-powder extrusions of high strength aluminium–copper–magnesium (–manganese or –zirconium) based alloys containing 1 to 3 wt % lithium can show better combinations of strength and ductility than similar compositions wrought from ingot [136]. Goals include an alloy with a 30% increase in specific modulus and one with 20% increases in both specific modulus and specific strength, compared to 7075-T76, to be achieved without significantly impairing other properties. It has been estimated that fuel consumption could be halved for an average aircraft if full advantage could be taken of reduced density and increased modulus combined with high strength in such alloys. Such improvements through extended alloying aided by RSR-processing are additional to worthwhile improvements in strength, plasticity, fatigue and stress corrosion performance obtainable by RSR-processing of conventional high strength wrought ingot alloys such as 2024, unaided by further alloy additions [132, 133, 160, 161]. The argument that such improvements should be attainable by ingot processing of material of sufficiently high purity overlooks the increasing need to be able to recycle material of *lower*, rather than higher, purity. The tolerance of RSR-processing to high levels of what are normally considered to be damaging impurities (e.g. iron and silicon in aluminium, and, compared with levels in metallic glasses, phosphorous or boron in iron and nickel) is one of its most useful features. The ability of RSR-processing to achieve, from a charge of aluminium-based automobile scrap containing 9.6 wt % Si and 0.8 wt % Fe, tensile properties intermediate between those of wrought 6063-T6 and 2024-T4, has recently been demonstrated [162]. The composition in question would not have been acceptable even for castings, let alone as a basis for wrought ingot processing.

Strengths as high as 4.5 GPa [163] have been reported for metallic glasses, in spite of reductions of elastic moduli by some 20 to 40% compared with the crystalline state. These high strengths ($\sim E/50$) with corresponding hardness and wear resistance (Section 4.2) can be combined with ductile behaviour in bending, shear and compression, although embrittlement can occur on annealing, and tensile ductility is invariably low. Exceptional corrosion resistance with high strength can be conferred by additions of such as chromium and phosphorus (Section 4.4) and thermal stability can be improved by adding or basing compositions on refractory metals (Section 4.3). Fracture toughness, although low, is two orders of magnitude larger than for silica glass and is higher than for high strength crystalline steels of the same yield strength. Fatigue life is normally much shorter than for such steels because there is no equivalent of work-hardening to disperse localized slip and so extend the time required for nucleation of fatigue cracks. This can amount to 90% of the time to failure for crystalline steels. The shorter fatigue life could be a considerable restriction in several proposed high-strength applications [164] involving cyclic stresses such as high-strength control cables, pressure vessels, flywheels for energy and power storage, mechanical transmission belts, torque transmission tubes and reinforcing elements for rubber tyres. Such applications, advanced mainly with continuous melt-spun ribbon in mind, as well as possibilities involving particulate, require an element of consolidation or bonding of the metallic glass to be achieved without significant degradation of properties. In particular, bonding must be achieved at temperatures below that for crystallization (T_x). Although some success in achieving densification and bonding while retaining the glassy structure has been reported for both uniaxial die pressing and extrusion at temperatures approaching T_x [165, 167], bonding and consolidation at even lower average temperatures has been achieved via dynamic cladding or compaction using explosive charges or a gas-gun. Temperature rises during consolidation can then be localized at the surfaces to be bonded so that, even if local melting occurs, it will be confined to such a narrow zone that the metallic glass can reform there on solidification as a result of rapid heat extraction into the unheated bulk of the material. Consolidates of PdCuSi and FeNiPB metallic glasses have been made [169–175] and cladding of NiFeB glass on to a steel has been achieved [169] by such techniques. In a similar way, ultrasonic welding has been used to bond FeNiPB glass to copper [176]. It would be even more satisfactory to achieve *in situ* bonding simultaneously with glass formation. Bonded bimetallic ribons of two different metallic glasses or of a glass and a crystalline material have been made via melt-spinning by using a second nozzle to deposit the second material on the solidified ribbon of the first material before it

has left the chill-block [177, 178]. Multilayer thick deposits of one material can be produced from a single nozzle by ensuring that the ribbon does not separate from the rotating chill-block [179]. Plasma-jet and flame-spraying have been used to form metallic glass deposits several hundred micrometres in thickness and approximately 80% to 90% dense [180–183]. Production of even thicker deposits at full density without loss of the glassy structure would significantly improve prospects for structural applications. An alternative to direct consolidation is to bond metallic glass ribbon or fibre in a suitable matrix. Good results have been obtained with epoxy resins [184–187] and more recently with a metal matrix of aluminium–calcium–zinc alloy which is superplastic at the temperature of consolidation (750 K), well below the crystallization temperature of the $Ni_{60}Nb_{40}$ metallic glass being bonded [188, 189]. The effectiveness of even small amounts of metallic glass in reinforcing mortar and cement has been demonstrated [190, 191] and the commercial benefits of introducing melt-extracted microcrystalline steel fibre into concrete to increase tensile and impact strength and resistance to wear and spalling have been pointed out [192].

4.2. Tool and bearing materials

Tool and bearing materials have in common the need to sustain adequate performance and durability under conditions that are liable to induce excessive wear in an unsuitable material. Tool and bearing steels have been a particular target of RSR-processing because they are notoriously difficult to process via the wrought ingot route, typical yield losses of 50 per cent adding substantially to production costs. These steels contain substantial amounts of hard and brittle eutectic carbides produced by segregation during ingot solidification and remaining as banding even after 98% reduction by hot-working. The use of RSR-processing to improve tool steels was first reported in the 1960s (e.g. [193]), typically involving extrusion of canned atomized alloy powder. The ensuing commercial developments employed inert gas or nitrogen atomization to generate spherical particulate subsequently densified by hot-isostatic-pressing to provide billets for rolling or forging to shape. Such procedures have been established in the USA, in Sweden and now in Japan to produce, respectively, *CPM* [194, 195], *ASP* [196] and *KHA* [197] high-speed steels. The fine dendrite spacing of a few micrometres and absence of coarse carbides in the atomized powder ensures a relatively uniform distribution of fine carbides during processing and in service. Processing advantages then include [194–198]:

1. elimination of the large hot-working reductions that are required to reduce sufficiently the scale of banding derived from ingots.
2. improved hot-workability allowing increased carbon and alloying levels to be considered.
3. more consistent machinability in the annealed condition and much improved grindability (due to absence of coarse carbides which increase resistance to *abrasive* wear), especially in highly alloyed steels.
4. accelerated austenitizing and hardening responses.
5. more consistent and predictable dimensional changes during heat treatment, allowing treatment to higher hardness without unacceptable distortion or cracking.

Furthermore, the finer and more uniform carbide distribution (Fig. 22), together with the smaller grain size obtained by heat treatment, are essentially independent of product size. This results in greater consistency and less directionality of properties in general, and improved toughness in particular. Benefits in service include increases in tool life in intermittent cutting operations (in which resistance to *adhesive* wear is paramount) by factors as large as five, as well as increased serviceability in working operations. Penetration of these P/M high speed steel products into markets currently occupied by conventional tool steels has been limited mainly by production costs associated with the hot-isostatic-pressing step in processing. Alternatives explored commercially include cold pressing and sintering [199] or extrusion [200] of cheaper and more compressible water-atomized powder, although coarsening of carbides at the high sintering temperatures required and retention of some porosity limits sintered products to less demanding applications [201, 202]. This is another instance where combining rapid solidification and consolidation in one operation would be advantageous in avoiding the economic and other penalties of producing and handling powder. Such a process [12] is reported to produce 96% to 98% dense material in substantial thicknesses by continuously depositing tool steels droplets ~ 1 mm in diameter on to a moving water-cooled collector. The droplets

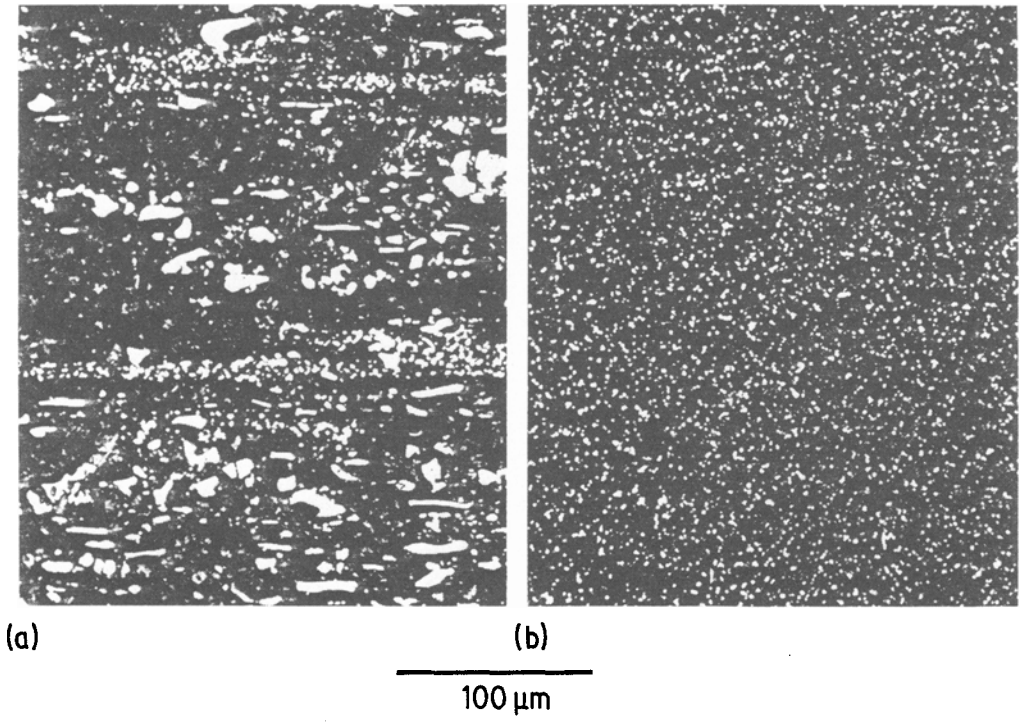

Figure 22 Effect of RSR-processing on carbide particle size and uniformity of distribution in type T15 tool steel. (a) Wrought ingot; (b) wrought from atomized alloy powder [194].

spread on deposition to give dendrite spacings as small as 1 μm in the deposit, indicating that cooling rates during solidification can approach 10^6 K sec^{-1}. The resulting *CSD* (Controlled Spray Deposition) steels generated by hot-working and heat treatment of the deposits do appear to retain the merits of P/M tool steels but by a more direct and so more economic route, not excluding the quality advantages that are especially important for higher alloyed grades in larger product forms.

A different approach using metallic glass as precursor material has been introduced recently [203–213]. This can involve formation of the metallic glass as melt-spun ribbon. This is followed, if necessary, by heat-treatment of the ribbon so as to induce embrittlement, then pulverization of the embrittled ribbon into fine powder, and finally consolidation by hot-isostatic-pressing or extrusion at a temperature inducing devitrification to produce a fine-grained ($\sim 0.25\ \mu$m) crystalline matrix stabilized by ~ 25 vol% borides or carbides of particle size $\sim 0.15\ \mu$m. Potential applications of such *pyromets* [214] include hot-work die tools requiring hot strength and hardness up to 650° C, oxidation resistance to 700° C and good impact resistance up to 540° C. Such materials arose from the development of metalloid-lean (5 to 13 at%) metallic glasses (contrasting with the 15 to 25 at% metalloid addition employed previously to stabilize such glasses). Thus the metalloid addition here serves the dual purpose of promoting glass formation in the first instance and then, as carbide or boride particles, stabilizing the fine matrix grain size that results from devitrification. One such product developed as a tool material has essentially the composition of M2 high speed steel with an addition of 1.1 wt% boron along with the 0.85 wt% carbon normally present. The earliest trials [203] on nickel–molybdenum–boron based compositions demonstrated considerable extensions in cutting-tool life compared with conventional M42 tool steel, doubling of the die life of a mould gate for aluminium die-casting ($>$ 116 000 shots as compared with 50 000 for H-13 steel) and trebling of the die life of a copper extrusion die compared with conventional high-cobalt rexalloy or stellite 6.

A further approach to improvement of wear resistance is to employ directed-energy-processing to incorporate carbides and borides directly into

a thin molten zone at the surface. The carbides/borides can be introduced, for example, by first plasma coating them on to the surface [215] or by direct injection into the melt pool as it is formed [216–218]. Wear resistance can thus be improved by at least an order of magnitude, making the treatment attractive for improving life of components such as automotive engine valve seats or chain-saw teeth [219]. Significant improvements in wear resistance of certain materials can be achieved by such laser or electron-beam surface treatment even in the absence of a surface alloying addition. Examples extend from forming white-iron on grey-iron automotive camshaft lobes [219] to remorphologizing the surface microstructure of a cemented carbide, the latter treatment extending the wear life by as much as three times [219].

4.3. High-temperature materials

The improvement of high temperature properties is an ever present goal of materials development and the potential of RSR-processing for that purpose has received attention from the outset. The pioneer work of Alcoa and Kaiser referred to in Section 4.1 established that hot strengths of atomized alloy powder extrusions of aluminium alloys containing substantial additions of transition metals were notably superior to those of conventional wrought aluminium alloys at temperatures above 200° C. This is attributable to the increased thermal stability of the submicron dispersion of low-solubility, low-solute-diffusivity aluminide intermetallics generated by rapid solidification, compared with the relatively soluble and high-solute-diffusivity precipitates produced by ageing in conventional alloys. The aluminium 8 wt % iron base composition established by these earlier studies has been the starting point for subsequent developments. Room temperature strength can be further increased by first generating a supersaturated solid solution [88], rather than an intermetallic dispersion, at the rapid solidification stage. This, combined with a lower consolidation temperature, resulted in doubling of room temperature strength to 570 MPa, the strength advantage being maintained up to at least 400° C [132]. The additional benefits of ternary additions such as zirconium, cerium, molybdenum and chromium in further improving thermal stability are evident in Fig. 23 [136]. Their effectiveness probably arises partly from their having lower diffusivities in aluminium, though reliable measurements do not exist for cerium and molybdenum. A different approach is to base alloy development on major additions of such as chromium and zirconium, known to have lower diffusivities in aluminium than for example iron, cobalt or nickel solutes. Decomposition temperature for the extended solid solution can then be raised as high as 490° C for aluminium–chromium [221], a remarkable advance on the ~ 150° C typical of conventionally solution-treated wrought alloys. The benefits of this extra stability can be seen in Fig. 23 for Al–6 wt % Cr–1 wt % Fe made by vapour-deposition [222]. It is not known yet whether such results can be matched by RSR-processing of this alloy. Examples of potential applications that could make use of the superior high-temperature properties of such materials include turbine fan blades and automotive pistons. RSR-processed Al–8 wt % Fe–2 wt % Mo is claimed [223] already to have a specific strength equal to the conventional Ti–6 Al–4 V alloy in current use for compressor blades.

Alloys for the hottest section of gas turbines are typically superalloys based on nickel, including relatively simple compositions for rolling into formable sheet, more complex alloys for forging into discs, together with the most highly-alloyed compositions limited to precision casting into blades [224]. The first developments using RSR-processing have been directed towards the turbine disc, principally involving hot-isostatic-pressing of atomized alloy powder, in parallel with the corresponding developments for tool steels discussed in Section 4.2. Corresponding advantages over ingot processing include [225]:

1. ability to form a part nearer to final shape by a shorter route with economies in input material and in final machining, resulting in cost savings as high as 50% to 60%.

2. improved hot-workability due to absence of macrosegregation and presence of a uniform fine dendritic microstructure and grain size, allowing previously non-forgeable compositions to be rendered hot-workable and even superplastic.

3. improved machinability and machine tool life due to elimination of massive carbides.

4. insensitivity both of processing variables and of final properties to billet size, with none of the defects associated with large cast superalloy ingots.

As well as facilitating production, RSR-processing overcomes limitations in properties, such as low

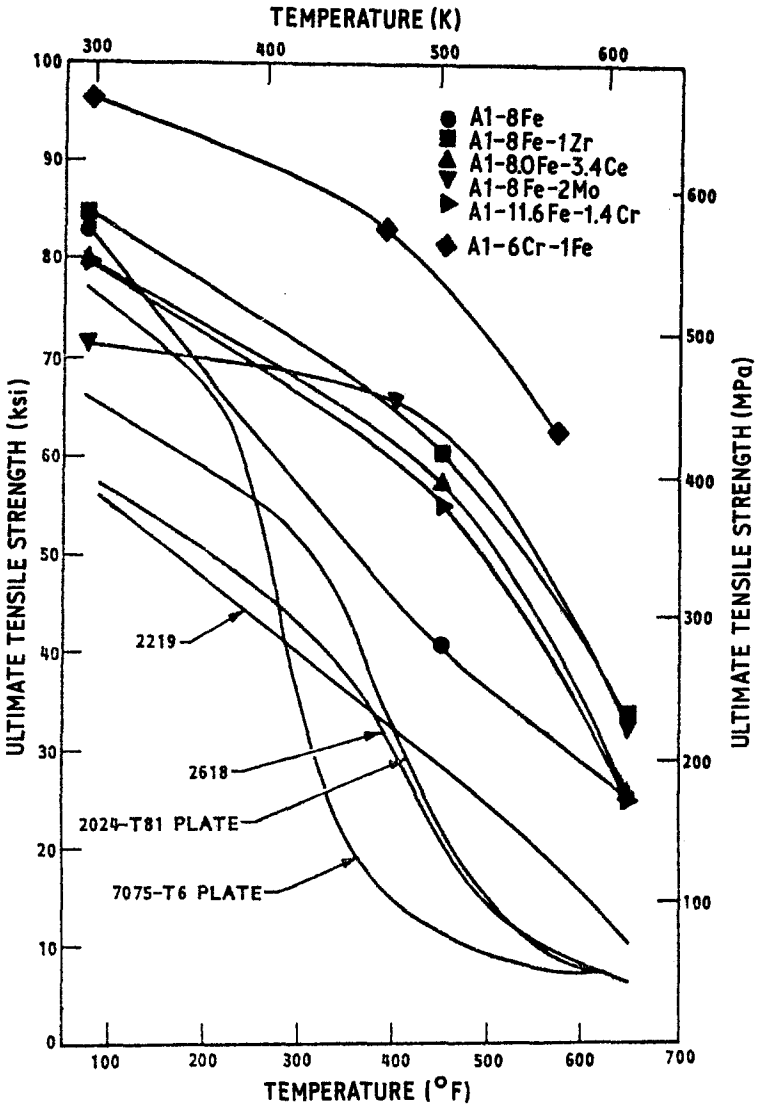

Figure 23 Ultimate tensile strength as a function of test temperature for RSR-processed Al–Fe based and vapour deposited Al–Cr based alloys compared with conventional wrought Al–Cu and Al–Zn based high-strength alloys [136]. Published by kind permission from T. E. Tietz and I. G. Palmer, Advanced P/M Aluminium Alloys in "Advances in Powder Technology", edited by G. Y. Chin (American Society for Metals, Metals Park, Ohio, 1982) p. 214.

cycle fatigue, of the cast or wrought ingot forms of alloys such as Astroloy, IN 100 or Rene 95 [226]. Advantage can then be taken of the higher strength provided by such alloys compared with the strongest conventional wrought alloy, Waspaloy, in present use for discs. Control of formation of carbide films at prior powder particle boundaries and of entrapment of argon or refractory particles from the atomizing process is essential for achievement of required properties in the final product. Attention has also been given to the use of RSR-processing in relation to turbine blades. Adequate creep rupture life at the higher temperatures involved (~ 1000° C) can be obtained in this case only by developing a relatively coarse grain structure from the fine grain size characteristic of RSR-processing. RSR-processed compositions based on Ni–17 wt % Al with 9 to 11 wt % molybdenum or chromium then show increases in temperature capability of up to 85° C (Fig. 24) in respect of creep strength with the molybdenum addition and in oxidation resistance by a factor of ten with the chromium addition compared with the strongest unidirectionally solidified alloy (MAR-M200 + Hf) in current use as a blade material [227]. Such RSR-compositions are not usable in cast or wrought ingot form because of unacceptable segregation and related effects, and so are a clear instance of extension of the limits of alloying by rapid solidification. The added possibility of fabricating via RSR-processing a wide range of superalloy compositions in the form of thin sheet is an essential element in the development of wafer-blade technology (Fig. 25) in which the turbine blade is

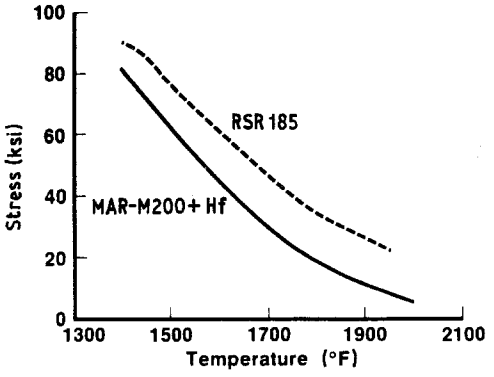

Figure 24 Stress to give 1% creep strain in 1000 h as a function of test temperature for an atomized powder extrusion of Ni–Al–Mo alloy compared with strongest currently-used unidirectionally-solidified alloy [227].

made by precision bonding of stacked arrays of wafers on the surfaces of which cooling passages have already been imprinted by photochemical etching [228]. The resulting combination of improved cooling efficiency with the higher temperature capability of RSR-alloys should permit higher turbine inlet temperatures, giving greater thrust to weight capability or alternatively longer engine life at current inlet temperatures.

The assembly of a complex piece of engineering equipment, such as a gas turbine, involves precision joining of parts. Current practice in choice of alloys for braze assembly of gas turbine components favours nickel-based alloys containing sufficient added boron, silicon, carbon or phosphorous to cause fusion at ~900 to ~1100° C. As normally cast, these alloys contain sufficient coarse and brittle second phase to render them non-workable, so they are mechanically pulverized and applied bonded with 50% of organic binder in the form of transfer tape. Use of such tape gives joints of variable integrity and strength due to

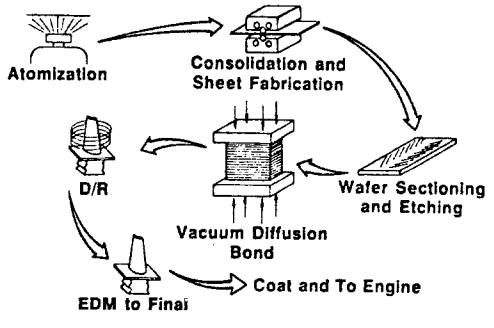

Figure 25 Proposed route for production of wafer turbine blades from rapidly solidified particulate [228].

incomplete accommodation of loss of binder during the braze cycle and inevitable variability of local composition of the braze powder itself. Many of these standard compositions can, however, be readily produced as continuous metallic glass foils by techniques such as planar flow casting [229]. Such foils have enough ductility to be formable to match part contours and can be cut or stamped to the required shape, thus minimizing waste. Their uniform composition results in more uniform melting and better control of penetration between parts, with enhanced dissolution of base metal and diffusion of braze metal. This, their uniform thickness of about one-third that of transfer tape, and the absence of organic binder, results in narrower, stronger, more ductile and more corrosion-resistant joints and shortens, simplifies and reduces variabilities in assembly. Corresponding braze compositions can be made as metallic glass foil on alloy bases other than nickel as required [230, 231] and there seems to be no reason why even a fully microcrystalline structure should not be adequate provided that it is not brittle, nor indeed why RSR-processing should not be widely applied to produce homogeneous brazing or welding alloy feedstocks in foil, wire or powder forms in addition to the metallic glass brazing foil already available commercially.

Such metallic glass brazing foils are essentially being used as precursor materials since they resolidify in *crystalline* form to form the brazed joint itself. In that sense they are analogous to the "pyromet" metallic glass precursor materials used to produce, on devitrification, microcrystalline materials suitable for tool and bearing applications as described in Section 4.2. Evidently the same approach can impart thermal stability via the high volume fraction of small-diameter dispersoid particles produced by devitrification, an important consideration in the example of hot-work die materials cited in Section 4.2. The limiting service temperature would then be determined by the resistance to coarsening shown by the dispersoid. A similar limitation has been noted [232–234] for the fine dispersion of additional titanium carbide afforded by RSR-processing of titanium-modified type 316 stainless steel which is effective in reducing swelling under irradiation conditions by providing significantly more sites for helium bubble precipitation. This is an important requirement in such an austenitic stainless steel under consideration as a candidate first-wall

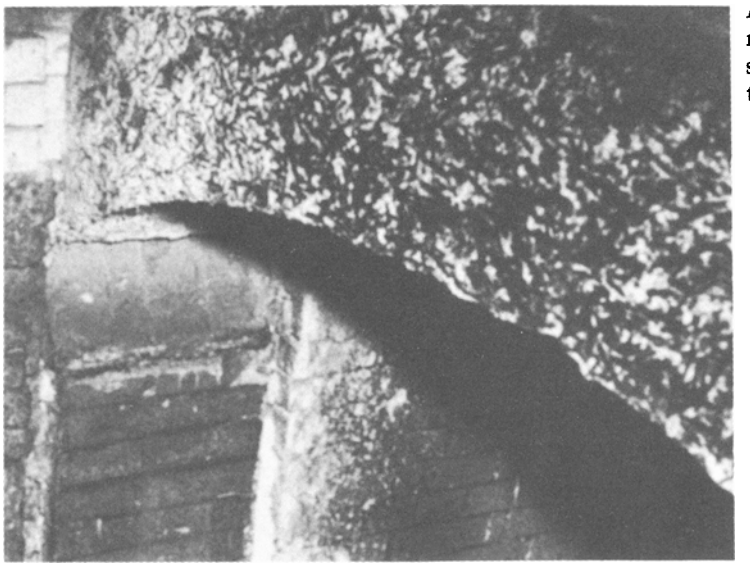

Figure 26 Pre-cast refractory furnace arch reinforced with melt-extracted type 302 stainless steel staples showing three times the life of unreinforced refractory [236].

material for fusion reactors. Attempts are being made to introduce a more stable oxide dispersion by adding 1 wt % Al to form dispersed surface alumina in RSR-powder feedstock when this is subjected to attrition under isopropyl alcohol [235]. This combination of RSR-processing with mechanical alloying has interesting possibilities for further development of high temperature alloys. Stainless steel also features in an established tonnage application of RSR-processing in a high temperature material – that of employing melt-extracted staples for reinforcement of industrial refractories. Manufacture of staples by melt-extraction halves their cost compared with conventional shear cutting and embossing of wrought material, while extending refractory life at 1650° C (Fig. 26) by factors of 2 or 3 [236].

4.4. Corrosion-resistant, catalytic and storage materials

The high resistance to corrosion exhibited by metallic glasses containing chromium and phosphorus (Fig. 27, [237, 238]) suggests a variety of marine, chemical and biomedical uses, for example, naval aircraft cables, torpedo tubes, chemical filters and reaction vessels, electrodes, razor blades and scalpels, suture clips, etc. [164]. The combination of corrosion resistance, high hardness and high magnetic induction offered by such an iron-based metallic glass used as a filter has been claimed to increase the rate of collection of magnetic and ferric hydroxide particles by a factor of three compared with a conventional ferritic stainless steel filter [239]. The corrosion resistance/hardness combination along with ability to be sharpened into a cutting tool underlies possible application as a long-life razor blade or surgeon's scalpel. Similarly for microcrystalline alloys, it has been claimed that the generally poor corrosion resistance of commercial Ag–Sn–Cu alloy dental amalgams can be improved in amalgams made from melt-spun alloy with increased copper content [240]. In addition, higher strength and ductility is obtained

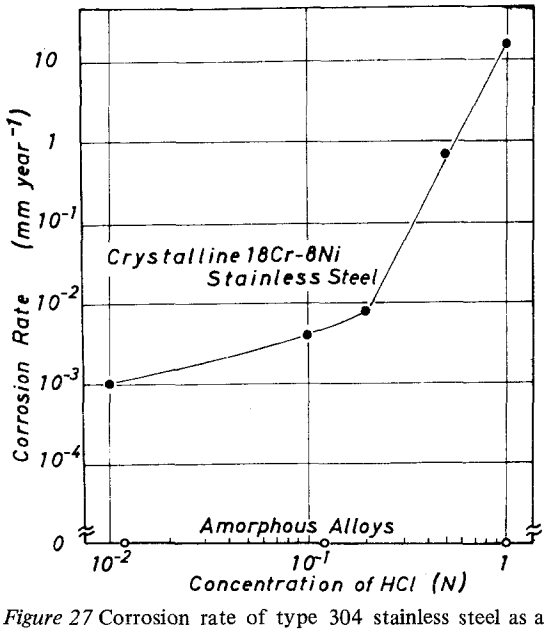

Figure 27 Corrosion rate of type 304 stainless steel as a function of HCl concentration at 30° C compared with zero detectable rate for Fe–Cr (–Ni)–P–C metallic glass after immersion for 168 h [237, 238].

compared with normal chill-cast alloy as a result of smaller grain size [241]. Extrusions of RSR-processed Al–6 to 8 wt % Fe alloy with additions of chromium, manganese and magnesium are reported [242] to exhibit resistance to corrosion in seawater exceeding that of conventional resistant Al–Mn and Al–Mg wrought ingot alloys. Combined with superior hot strength, thermal conductivity and low cost compared with established copper–nickel alloys, this suggests applications as condenser and heat-exchanger tubing in desalination plants. Corrosion and/or oxidation resistance combined with strength at elevated temperature is also claimed [207, 208, 210, 212, 213] for boride/carbide dispersion-stabilized austenitic stainless steels and nickel-base alloys made from metallic glass precursors as described in Section 4.2, and for ferritic steels containing levels of aluminium usually prohibited to wrought-ingot processing because of inadequate ductility [243, 244]. The resistance to oxidation [245] and to corrosion [246] of stainless steels of conventional composition has been reported to be improved by RSR-processing, attribute to refinement of inclusions and matrix grain size. Such improvements correspond to those in resistance to corrosion and stress-corrosion obtained by RSR-processing of conventional high-strength aluminium alloy compositions developed for wrought-ingot processing (Section 4.1). The use of directed-energy processing to produce a rapidly-solidified corrosion-resistant layer at surfaces has also been investigated. Benefits include restoration of protection against intergranular attack to sensitized type 304 stainless steel [247] and increased resistance to attack by chloride solutions of type 614 aluminium bronze [248], both effects attributed to the homogenizing effect of the RSR-treatment applied. Trials on the production of corrosion-resistant metallic glass layers on mild steel [249] and nickel [250], by laser fusion of a prior deposit of the required composition, have been reported.

The catalytic and gas-storage capabilities of RSR-processed materials have also received attention. Iron–nickel–phosphorous(–boron) metallic glass ribbon has been reported to be a hundred times more effective in catalysing the hydrogenation of carbon monoxide to yield hydrocarbons, than its crystalline form [251–253]. Surface-activated palladium-based metallic glasses were reported to exhibit catalytic activities for oxidation of methanol, sodium formate and formaline similar to or higher than platinized platinum, suggesting application as an electrode material for a methanol–air fuel cell [254]. Palladium-based metallic glasses also show particularly high electrocatalytic activity for chlorine evolution in hot concentrated NaCl solutions, while retaining high corrosion resistance, suggesting application as a corrosion-resistant energy-saving anode in the electrolytic soda process [255]. Such enhanced catalytic behaviour is not confined to metallic glasses among rapidly-solidifed materials. Activated microcrystalline Al–30 to 50 at % Ni rapidly-solidified powders were reported to be more effective for catalysing hydrogenation of a series of organic compounds than were the same alloys in conventional cast form [256].

The advantages of metallic glasses as storage materials for hydrogen, compared with corresponding crystalline intermetallic compounds, include larger capacity, wider composition range and higher ductility. A number of metallic glasses containing hydride-forming elements, e.g. Cu–Ti, Zr–Ni and Ti–Ni, are under evaluation [257–264]. Applications include storage of hydrogen as a fuel for vehicles, heat pumps and air-conditioners [262].

4.5. Electrical and magnetic materials

The report by Duwez and Lin [265] in 1967 of typical soft ferromagnetic behaviour for Fe–15 at % P–10 at % C metallic glass heralded a major new field of research in magnetism, and indeed, on the basis of number of published papers, *the* major research activity to date in the entire field of RSR-processing. Conventional metallic soft magnetic materials range from low-cost common iron and silicon iron used in large volume mainly for cores of power transformers and motors, to relatively costly nickel and cobalt irons used in smaller volumes in electronic devices. Transformer cores and motors use material in the form of sheet ~ 0.3 mm in thickness while electronic equipment uses tape 25 to 100 μm in thickness. This sheet and tape is wrought from ingot feedstock by lengthy sequences of rolling with intermediate anneals designed to control crystallographic texture and thereby properties. Such costly fabrication procedures contrast with the relatively simple and inexpensive techniques of melt-spinning and planar-flow casting which produce ferromagnetic metallic glasses in the form of continuous ribbon and wide tape at high speed

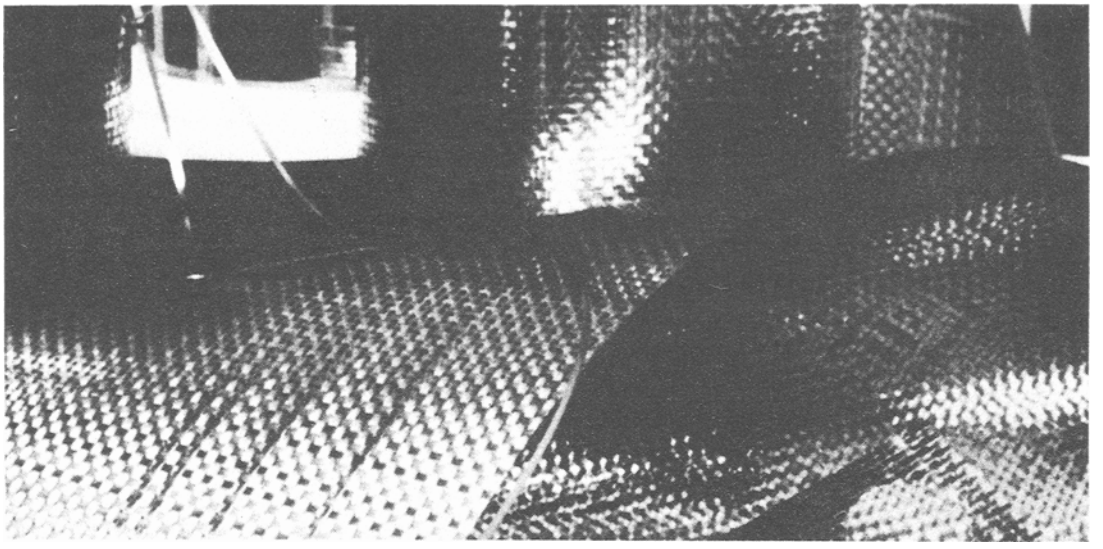

Figure 28 Flexible magnetic shielding woven from metallic glass melt-spun ribbon (from W. K. Kinner, *Materials Engineering* 89 (1) (1979) 32).

in one step directly from the melt. In addition, their high electrical resistivity and low coercivity reduce core losses under a.c. excitation to levels typically one-third those of the best oriented silicon iron, while achieving at Ni : Fe ratio ~ 1 : 1, in the presence of metalloids, properties comparable to permalloys with Ni : Fe ratios of 5 : 1, thereby economizing on relatively costly nickel, in particular [266–268]. Energy savings resulting from low core losses are the main incentive for substituting metallic glass for silicon iron in power devices while cost savings are the main attraction for applications in electronic devices. The first *electronic* application was of Fe–Ni–P–B metallic glass ribbon braided or woven into continuous fabric up to 2 m wide for use as *magnetic shielding* material (Fig. 28) with the advantage over conventional permalloy of being formable into the required shape without impairment of shielding performance [269, 270]. The limited shielding efficiency of Fe–Ni–P–B is reported [271] to be improved by using more costly cobalt-based metallic glasses with higher initial permeability and zero magnetostriction. Another electronic application taking advantage of high permeability, this time with high electrical resistivity, mechanical hardness, and resistance to corrosion and wear, is for *recording/replay or read/write heads* for audio, video, computer or instrumental recording machinery. High flux density and wear resistance improve audio response and life, respectively, to give overall performance claimed to be superior to conventional crystalline ferrites, permalloys and sendust [272]. Other electronic applications include acoustic delay lines, transversal filters, stress or temperature transducers or sensors, current transformers, leakage and overcurrent alarms, analogue-to-digital convertors, small-power wattmeters and in switched mode power supplies [266–268, 271, 273]. While the number and variety of such electronic applications already devised is certainly impressive, proposed applications in *power devices*, especially as core materials in power transformers and motors, are even more significant. It has been estimated [273] that reduction in core losses from 1.5 to 0.44 $W kg^{-1}$ by substituting iron–boron metallic glass for oriented silicon iron would save $200 million annually in the USA now wasted as heat in distribution transformers. Although the reduction in saturation flux associated with the metalloid additions is a potential drawback of such metallic glasses, this has become less important with the trend to operate silicon iron cores at lower flux densities to reduce losses [268]. The reduced sheet thickness of the metallic glass could also be a disadvantage if it reduced the packing fraction attainable in wound or stacked cores and structures. It has been suggested [268], however, that if conventional silicon iron sheet could be made as thin as metallic glasses without loss of preferred orientation, core losses could be as low as for

metallic glasses. Recent developments [274] have shown that this is indeed the case for crystalline silicon irons with double the normal silicon content made by direct casting from the melt followed by heat treatment to develop crystallographic texture. The reduction of ductility associated with such high silicon contents prohibits production by rolling of ingot material, so this is another example of beneficial extension of alloying by RSR-processing.

The high electrical resistivity of metallic glasses is comparable with established crystalline resistance alloys such as nichrome, suggesting applications as precision resistors, high-strength low-temperature heating elements or radiation-resistant low-temperature thermometers [275]. Pd–Cr–Si [276] and Ti–Zr–Be [277] based metallic glasses have been proposed for the thermometric purpose. Poor workability limits conventional wrought resistor alloys based on Fe–Cr–Al to levels of chromium and aluminium less than 15 and 16 at %, respectively. Higher resistivity with zero temperature coefficient has been obtained [278, 279] for melt-spun microcrystalline alloys at levels of chromium and aluminium of 30 and 15 at %, respectively, with the added bonus of high strength and good ductility, another instance of useful extension of alloying via RSR-processing. Uniformity of field-emission from metallic glasses suggests uses as electron sources in electron-optical equipment [280] while their reproducible glass transition temperature might be useful in an electrical fuse material [281]. The resistance to radiation of superconducting metallic glasses could lead to applications in large superconducting magnets required for fusion technology [282]. Partial crystallization of a metallic glass has been reported to improve markedly superconducting properties while retaining good ductility [283–285]. Concerning more conventional conductor materials, the use of the Taylor wire method to generate glass-sheathed small-diameter copper conductors for electrical circuits and composites has been proposed [286, 287] and the application of RSR-processing to disperse hard second phases of low solid solubility through high-conductivity metals, so as to increase strength with minimal impairment of conductivity, has been applied to both copper [288, 289] and aluminium [290, 291]. Incorporation of 8 vol. % melt-extracted aluminium fibres into polymers to impart sufficient conductivity for them to carry house currents and to render them effective as electromagnetic shielding materials has been reported [33].

5. Conclusion

Rapid solidification technology (RST) is evidently now in the position of being able to offer a wide variety of product forms for a wide range of possible applications. Although notable progress is being made in successfully modelling both the processing and materials science aspects of RST, many unresolved questions remain to challenge the scientific community at large. The effect of RSR-processing conditions on both structure and properties still needs to be fully characterized and, in particular, much scope remains for carefully controlled studies to define and elucidate underlying relationships. Current developments related to applications indicate that any polarization between alternatives such as production by atomization as opposed to melt-spinning or formation of metallic glass as opposed to extended crystalline solid solution to achieve useful final products forms and properties, is less apparent than it was even five years ago. That is one indication that the subject has moved from infancy in the 1960s through adolescence in the 1970s into maturity in the 1980s. The task of the 1980s is to make sure that the promise of RST is realized *wherever* it can bring nearer the achievement of objectives of research programmes and promote more efficient processing, or better products, in industry. Whatever the outcome of such activities, the future of RST evidently is not identifiable with any single process, activity or application as shown by its penetration over a relatively short period into most of the major fields of study or application of metallic materials. Whichever of the current developments and applications turns out to be most significant, the scientific and technological questions they raise will undoubtedly continue to fascinate and challenge for many years to come.

References

1. D. C. A. MOORE and D. R. GABE, *Trans. Inst. Met. Finish.* (1983) in press.
2. R. P. ALLEN, S. D. DAHLGREN and M. D. MERZ, in "Rapidly Quenched Metals", edited by B. C. Giessen and N. J. Grant (MIT Press, Cambridge, MA, 1976) p. 37.
3. P. DUWEZ, R. H. WILLENS and W. KLEMENT, *J. Appl. Phys.* **31** (1960) 1136.
4. P. DUWEZ and R. H. WILLENS, *Trans. Met. Soc. AIME* **227** (1963) 362.
5. H. JONES, "Rapid Solidification of Metals and

Alloys", (Institution of Metallurgists, London, 1982).
6. *Idem, Mater. Sci. Eng.* **5** (1970) 297.
7. *Idem*, in "Rapid Solidification Processing: Principles and Technologies", edited by R. Mehrabian *et al.* (Claitor's Publishing Division, Baton Rouge, LA, 1978) p. 28.
8. A. R. COX, J. B. MOORE and E. C. VAN REUTH, in "Superalloys: Metallurgy and Manufacture", edited by B. H. Kear *et al.* (Claitor's Publishing Division, Baton Rouge, LA, 1976) p. 45.
9. V. ANAND, A. J. KAUFMAN and N. J. GRANT, in "Rapid Solidification Processing: Principles and Technologies II", edited by R. Mehrabian *et al.* (Claitor's Publishing Division, Baton Rouge, LA, 1980) p. 273.
10. J. PEREL, J. F. MAHONEY, B. E. KALENSHER and K. E. VICKERS, in "Rapid Solidification Processing: Principles and Technologies", edited by R. Mehrabian *et al.* (Claitor's Publishing Division, Baton Rouge, LA, 1978) p. 258.
11. A. R. E. SINGER, in "Advanced Fabrication Processes", Proceedings of the Agard Conference 256, Florence 1978, Paper 19.
12. B. A. RICKINSON *et al., Powder Met.* **24** (1981) 1.
13. M. H. KIM and H. JONES, in "Rapidly Quenched Metals" Vol. I, edited by T. Masumoto and K. Suzuki (The Japan Institute of Metals, Sendai, 1982) p. 85.
14. E. A. STRANGE and C. H. PIM, US Patent 905758 (1908).
15. M. C. NARASIMHAN, US Patent 4142571 (1979).
16. D. LA W. KING, US Patent 3522036 (1970).
17. R. E. MARINGER and C. E. MOBLEY, *J. Vac. Sci. Technol.* **11** (1974) 1067.
18. B. H. KEAR, J. W. MAYER, J. M. POATE and P. R. STRUTT, in "Metallurgical Treatises", edited by J. K. Tien and J. F. Elliott (Metals Society of the American Institute of Mechanical Engineers, 1981) p. 321.
19. W. H. WALTON and W. C. PREWETT, *Proc. Phys. Soc.* **62** (1949) 341.
20. R. P. FRASER, J.-Y. JANG and J. C. MOLLENDORF, *J. Inst. Fuel* **36** (1963) 316.
21. H. LUBANSKA, *J. Metals* **22** (1970) 45.
22. M. H. KIM, Ph.D. Thesis, Sheffield (1982).
23. C. G. LEVI and R. MEHRABIAN, *Met. Trans. B* **11B** (1980) 21.
24. *Idem, Met. Trans. A* **13A** (1982) 221.
25. W. N. GILL, T. CHOH and M. INOUYE, *Chem. Eng. Commun.* **12** (1981) 3.
26. C. A. WILLIAMS and H. JONES, *Mater. Sci. Eng.* **19** (1975) 293.
27. K. MIYAZAWA and J. SZEKELY, *Met. Trans. B* **10B** (1979) 349.
28. Y. V. MURTY and R. P. I. ADLER, *J. Mater. Sci.* **17** (1982) 1945.
29. K. I. MIYAZAWA *et al.*, as [13] p. 73.
30. K. MIYAZAWA and J. SZEKELY, *Met. Trans. A* **12A** (1981) 1047.
31. J. ISHIHARA and I. IKUTO, as [13], p. 19.
32. S. R. ROBERTSON, T. J. GORSUCH and R. P. I. ADLER, as [7], p. 188.
33. R. E. MARINGER and C. E. MOBLEY, in "Rapidly Quenched Metals III" Vol. 1, edited by B. Cantor (The Metals Society, London, 1978) p. 49.
34. H. JONES, *J. Inst. Metals* **97** (1969) 38.
35. H. H. LIEBERMANN and C. D. GRAHAM, *IEEE Trans. Mag.* **Mag-12** (1976) 921.
36. S. J. B. CHARTER, D. R. MOONEY, R. CHEESE and B. CANTOR, *J. Mater. Sci.* **15** (1980) 2658.
37. S. KAVESH, in "Metallic Glasses" (American Society for Metals, Metals Park, Ohio, 1978) p. 36.
38. H. R. HILLMANN and H. R. HILZINGER, in "Rapidly Quenched Metals III" Vol. 1, edited by B. Cantor (The Metals Society, London, 1978) p. 22.
39. H. H. LIEBERMANN, *Mater. Sci. Eng.* **43** (1980) 203.
40. S-C. HUANG and H. C. FIEDLER, *Mater. Sci. Eng.* **51** (1981) 39.
41. *Idem, Met. Trans. A* **12A** (1981) 1107.
42. J. H. VINCENT, H. A. DAVIES and J. G. HERBERTSON, in "Continuous Casting of Small Sections", edited by Y. V. Murty and F. R. Mollard (Metals Society of the American Institute of Mining, Metallurgical and Petroleum Engineers, 1981) p. 103.
43. J. H. VINCENT, J. G. HERBERTSON and H. A. DAVIES, as [13], p. 77.
44. J. H. VINCENT and H. A. DAVIES, in "Solidification Technology in the Foundary and Casthouse" (The Metals Society, London, 1983).
45. J. H. VINCENT, J. G. HERBERTSON and H. A. DAVIES, *J. Mater. Sci. Lett.* **2** (1983) 88.
46. F. E. LUBORSKY and H. H. LIEBERMANN, *Mater. Sci. Eng.* **49** (1981) 257.
47. D. PAVUNA, *J. Mater. Sci.* **16** (1981) 2419.
48. D. C. AGRAWAL, *J. Mater. Sci. Lett.* **1** (1982) 385.
49. P. H. SHINGU, K. KOBAYASHI, R. SUZUKI and K. TAKESHITA, as [13], p. 57.
50. L. KATGERMAN *et al., Scripta Metall.*, **14** (1980) 861.
51. *Idem*, as [13], p. 61.
52. S. TAKAYAMA and T. OI, *J. Appl. Phys.* **50** (1979) 4962.
53. F. JACKSON, *Proc. Edinb. Math. Soc.* **14** (1964) 109.
54. N. CHRISTENSEN, V. DE, L. DAVIES and K. GJERMUNDSEN, *Brit. Welding J.* **12** (1965) 54.
55. Y. ARATA, F. MATSUDA and K. NAKATA, *Trans. Jpn Weld. Res. Inst.* **5** (1976) 47.
56. L. F. DONÀ DALLE ROSE and A. MIOTELLI, *Rad. Effects* **53** (1980) 19.
57. H. TONG and W. H. GIEDT, *J. Heat Transfer* **93** (1971) 155.
58. E. M. BREINAN, B. H. KEAR, C. M. BANAS and L. E. GREENWALD, as [8], p. 435.
59. H. E. CLINE and T. R. ANTHONY, *J. Appl. Phys.* **48** (1977) 3895.
60. S. C. HSU, S. KOU and R. MEHRABIAN, *Met. Trans. B* **9B** (1978) 221; S. CHAKRAVORTY and R. MEHRABIAN, **11B** (1980) 29.
61. P. BAERI, S. U. CAMPISANO, G. FOTI and E. RIMINI, *Appl. Phys. Lett.* **33** (1978) 137.
62. *Idem, J. Appl. Phys.* **50** (1979) 788.
63. J. C. WANG, R. F. WOOD and P. P. PRONKO, *Appl. Phys. Lett.* **33** (1978) 455.

64. R. F. WOOD, C. W. WHITE, B. R. APPLETON, P. P. PRONKO, S. R. WILSON and W. H. CHRISTIE, in "Laser–Solid Interactions and Laser Processing", edited by S. D. Ferris *et al.*, (American Institute of Physics, New York, 1979) p. 123.
65. R. TSU, R. T. HODGSON, T. Y. TAN and J. E. BAGLIN, *Phys. Rev. Lett.* **42** (1979) 1356.
66. *Idem*, in "Laser and Electron Beam Processing of Materials", edited by C. W. White and P. S. Peercy (Academic Press, New York and London, 1980) p. 149.
67. C. M. SURKO, A. L. SIMONS, D. H. AUSTON, J. A. GOLOVCHENKO, R. E. SLUSHER and T. N. C. VENKATESAN, *Appl. Phys. Lett.* **34** (1979) 635.
68. *Idem*, as [64], p. 155.
69. J. MUZUMDER and W. STEEN, *J. Appl. Phys.* **51** (1980) 941.
70. A. K. JAIN, V. N. KULKARNI and D. K. SOOD, *Appl. Phys.* **25** (1981) 127.
71. R. F. WOOD and G. E. GILES, *Appl. Phys. Lett.* **38** (1981) 422.
72. *Idem, Phys. Rev.* **23** (1981) 2923.
73. H. JONES, in "Treatise on Materials Science and Technology" Vol. 20, edited by H. Herman (Academic Press, New York, 1981) p. 1.
74. D. H. AUSTON, C. M. SURKO, T. N. C. VENKATESAN, R. E. SLUSHER and J. A. GOLOVCHENKO, *Appl. Phys. Lett.* **33** (1978) 437.
75. D. H. AUSTON, J. A. GOLOVCHENKO, A. L. SIMONS, R. E. SLUSHER, P. R. SMITH, G. M. SURKO and T. N. C. VENKATESAN, as [64], p. 11.
76. G. L. GALVIN, M. O. THOMPSON, J. W. MAYER, R. B. HAMMOND and P. S. PEERCY, quoted by J. M. Poate in "Laser and Electron Beam Interactions with Solids", edited by B. R. Appleton and G. K. Cellar (Elsevier, New York, 1982).
77. C. SURYANARAYANA and T. R. ANANTHARAMAN, *J. Mater. Sci.* **5** (1970) 992.
78. I. W. DONALD and H. A. DAVIES, *ibid.* **15** (1980) 2754.
79. B. C. GIESSEN, in "Advances in X-ray Analysis" Vol. 12, edited by C. S. Barrett *et al.* (Plenum, New York, 1969) p. 23.
80. B. C. GIESSEN, as [13], p. 213.
81. S. WHANG, *Mater. Sci. Eng.* **57** (1983) 87.
82. M. HAGIWARA, A. INOUE and T. MASUMOTO, *Met. Trans. A* **12A** (1981) 1027.
83. J. H. PEREPEZKO and J. S. PAIK, in "Rapidly Solidified Amorphous and Crystalline Alloys", edited by B. H. Kear *et al.* (Elsevier, New York, 1982) p. 49.
84. I. R. HUGHES and H. JONES, *J. Mater. Sci.* **11** (1976) 1781.
85. H. KOSUGE and I. MIZUKAMI, *J. Jpn Inst. Light Met.* **25** (1975) 48.
86. R. M. K. YOUNG and T. W. CLYNE, *Scripta Metall.* **15** (1981) 1211.
87. N. H. BURDEN and H. JONES, *Metallography* **3** (1970) 307.
88. H. JONES, *Mater. Sci. Eng.* **5** (1969) 1.
89. T. F. KELLY, G. B. OLSON and J. B. VANDER SANDE, as [83], p. 343.
90. M. H. BURDEN and H. JONES, *Fizika* **2** (Suppl. 2) (1970) Paper 17.
91. W. J. BOETTINGER, as [13], p. 99.
92. H. JONES and W. KURZ, *Met. Trans. A* **11A** (1980) 1265.
93. D. R. UHLMANN, *J. Non-Cryst. Solids* **7** (1971) 337.
94. H. A. DAVIES, as [33], p. 1.
95. *Idem, Rev. Chimie Minerale* **16** (1979) 349.
96. T. W. CLYNE, submitted to *Met. Trans.*
97. T. B. MASSALSKI, as [13], p. 203.
98. H. BILONI and B. CHALMERS, *Trans. Met. Soc. AIME* **233** (1965) 373.
99. M. HILLERT and B. SUNDMAN, *Acta Metall.* **25** (1977) 11.
100. J. C. BAKER and J. W. CAHN, *Acta Metall.* **17** (1969) 575.
101. *Idem*, in "Solidification" (American Society for Metals, Metals Park, Ohio, 1971) p. 23.
102. K. A. JACKSON and H. J. LEAMY, as [64], p. 102.
103. K. A. JACKSON, G. H. GILMER and H. J. LEAMY, as [66], p. 104.
104. R. F. WOOD, *Appl. Phys. Lett.* **37** (1980) 302.
105. S. U. CAMPISANO, G. FOTI, P. BAERI, M. G. GRIMALDI and E. RIMINI, *Appl. Phys. Lett.* **37** (1980) 719.
106. P. BAERI, J. M. POATE, S. U. CAMPISANO, G. FOTI, E. RIMINI and A. G. CULLIS, *ibid.* **37** (1980) 912.
107. P. BAERI, G. FOTI, G. M. POATE, S. U. CAMPISANO and A. G. CULLIS, *ibid.* **38** (1981) 800.
108. M. J. AZIZ, *J. Appl. Phys.* **53** (1982) 1158.
109. J. W. CAHN, S. R. CORIELL and W. J. BOETTINGER, as [66], p. 89.
110. C. W. WHITE, as [76], p. 109.
111. P. L. LUI *et al.*, *Appl. Phys. Lett.* **34** (1979) 864.
112. *Idem*, as [66], p. 156.
113. A. G. CULLIS, H. C. WEBBER, N. G. CHEW, J. M. POATE and P. BAERI, *ibid.* **49** (1982) 219.
114. J. M. POATE, in "Microsc. Semicond. Mater.", Inst. of Phys. Conf. Ser. No. 60, Section 2 (1981) p. 69.
115. *Idem*, as [76], p. 121.
116. W. W. MULLINS and R. F. SEKERKA, *J. Appl. Phys.* **35** (1964) 444.
117. A. G. CULLIS, D. T. J. HURLE, H. C. WEBBER, N. G. CHEW, J. M. POATE, P. BAERI and G. FOTI, *Appl. Phys. Lett.* **38** (1981) 642.
118. J. NARAYAN, as [76], p. 141.
119. J. NARAYAN and C. W. WHITE, as [83] p. 553.
120. R. J. SCHAEFER, S. R. CORIELL, R. MEHRABIAN, C. FENIMORE and F. S. BIANCANIELLO, as [83], p. 79.
121. S. R. CORIELL and R. F. SEKERKA, as [9], p. 35.
122. S. P. MIDSON and H. JONES, as [13], p. 1539.
123. W. J. BOETTINGER, as [83], p. 15.
124. P. RAMACHANDRARAO, M. G. SCOTT and G. A. CHADWICK, *Phil. Mag.* **25** (1969) 961.
125. C. G. LEVI and R. MEHRABIAN, *Met. Trans. A* **13A** (1982) 13.
126. C. J. BOUTEN, Thesis, Delft (1979).
127. J. D. HUNT, in "Solidification and Casting of Metals" (The Metals Society, London, 1979) p. 3.
128. W. KURZ and D. J. FISHER, *Acta Metall.* **29** (1981) 11.

129. D. J. FISHER and W. KURZ, *ibid.* **28** (1980) 777.
130. P. G. BOSWELL and G. A. CHADWICK, *Scripta Metall.* **11** (1977) 459.
131. R. E. SPEAR and G. R. GARDNER, *Trans. AFS* **71** (1963) 209.
132. H. JONES, *Aluminium* **54** (1978) 274.
133. M. LEBO and N. J. GRANT, *Met. Trans.* **5** (1974) 1547.
134. E. W. COLLINGS, C. E. MOBLEY, R. E. MARINGER and H. L. GEGEL, as [33], p. 188.
135. O. A. RUANO, L. E. EISELSTEIN and O. D. SHERBY, *Met. Trans. A* **13A** (1982) 1785.
136. T. E. TIETZ and I. G. PALMER, in "Advances in Powder Technology", edited by G. Y. Chin (American Society for Metals, Metals Park, Ohio, 1982) p. 189.
137. W. MARRIOTT, British Patent 3322 (1872).
138. P. F. COWING, US Patent 809671 (1906).
139. E. SMALL, US Patent 262625 (1882).
140. E. H. STRANGE, British Patent 20518 (1910).
141. R. H. WILLENS, E. BUEHLER and B. T. MATTHIAS, *Rev. Sci. Instrum.* **39** (1968) 194.
142. J. I. GOLDSTEIN, F. J. MAJESKE and H. YAKOWITZ, in "Advances in X-ray Analysis" Vol. 10, edited by J. B. Newkirk and G. P. Mallett (Plenum, New York, 1967) p. 431.
143. R. C. DORWARD, *J. Nucl. Mater.* **27** (1968) 235.
144. C. JANSEN, B. C. GIESSEN and N. J. GRANT, *J. Metals* **20** (1968) 10.
145. A. R. KAUFMANN and W. C. MULLER, in "Beryllium Technology" Vol. 1 (Gordon and Breach, New York, 1966) p. 629.
146. G. BEGHI, R. MATERA and G. PIATTI, *J. Nucl. Mater.* **26** (1968) 219.
147. *Idem, ibid.* **31** (1969) 259.
148. C. F. DIXON and H. M. SKELLY, *Int. J. Powder Metall.* **1** (1965) 28.
149. Anon., *Metals Society World* **2** (1983) 4.
150. R. S. BUSK and T. E. LEONTIS, *Trans. AIME* **188** (1950) 297.
151. S. J. ROBERTS in "Powder Metallurgy" edited by W. Leszynski (Interscience, New York, 1961) p. 799.
152. R. J. TOWNER, *Metal Progress* **73**(5) (1958) 70.
153. *Idem, Metals Eng. Q.* **1**(1) (1961) 24.
154. A. P. HAARR, ASTIA Reports AD 479783 and 487764 (1965–66).
155. J. P. LYLE and W. S. CEBULAK, *Met. Eng. Q.* **14** (1974) 52.
156. *Idem, Met. Trans. A* **6A** (1975) 685.
157. S. ASHLEY, *American Metal Market Metalworking News* **90** No. 100 (1982) p. 9.
158. S. J. SAVAGE and H. JONES, as [13], p. 159.
159. E. A. STARKE, T. H. SAUNDERS and I. G. PALMER, *J. Metals* **33**(8) (1981) 24.
160. D. P. VOSS, Research Report FB 79-34, DFVLR, Cologne (1979).
161. D. P. VOSS and W. BUNK, Proceedings of the 7th International Conference on Light Metals, Leoben/Vienna, June 1981 (Aluminium-Verlag, Dusseldorf, 1981) p. 229.
162. L. KATGERMAN, H. KLEINJAN, R. W. E. KROPF and W. G. ZALM, Proceedings of the 2nd International Symposium on "Materials and Energy from Refuse", Antwerp, October, 1981, edited by A. Buekens (KVIV, Antwerp, 1981) p. 5.7.
163. R. RAY, US Patent 4140525 (1979).
164. J. J. GILMAN, *J. Physique* **41** Suppl. 8 (1980) C8-811.
165. S. A. MILLER and R. J. MURPHY, as [9], p. 385.
166. *Idem*, as [13], p. 137.
167. H. H. LIEBERMANN, as [9], p. 393.
168. *Idem, Mater. Sci. Eng.* **46** (1980) 241.
169. C. F. CLINE and R. W. HOPPER, *Scripta Metall.* **11** (1977) 1137.
170. C. F. CLINE, J. MAHLER, M. FINGER, W. KUHL and R. HOPPER, as [7], p. 380.
171. C. F. CLINE, as [13], p. 129.
172. D. G. MORRIS, *Metal Sci.* **14** (1980) 215.
173. *Idem*, as [9], p. 372.
174. *Idem, J. Mater. Sci.* **17** (1982) 1789.
175. *Idem*, as [13], p. 145.
176. H. KREYE, H. YOSHINO and K. INOMATA, *Scripta Metall.* **12** (1978) 1059.
177. S. SHIMANUKI *et al.*, as [13], p. 15.
178. R. V. RAMAN and A. F. WITT, as [83], p. 141.
179. B. C. GIESSEN, S. DAVIS, S. W. HANG and B. H. KEAR, as [9], p. 237.
180. B. C. GIESSEN, N. M. MADHAVA, R. J. MURPHY, R. RAY and J. SURETTE, *Met. Trans.* **8A** (1977) 364.
181. P. H. SHINGU, K. SHIMOHURA and R. OZAKI, *Trans. Jpn Inst. Met.* **20** (1979) 33.
182. H. MIURA, S. ISA, K. OMURA and N. TANIGAMI, *ibid.* **22** (1981) 597.
183. H. MIURA, S. ISA and K. OMURA, as [13], p. 43.
184. D. J. GOLDWASSER and B. H. KEAR, *Mater. Sci. Eng.* **23** (1976) 237.
185. D. J. GOLDWASSER, E. P. OTOLKA and B. H. KEAR, *ibid.* **34** (1978) 139.
186. J. R. STRIFE and K. M. PREWO, *SAMPE J.* **16** (3) (1980) 8.
187. W. M. S. B. W. KADIR, C. HAYZELDEAN and B. CANTOR, *J. Mater. Sci.* **15** (1980) 2663.
188. S. J. CYTRON, *J. Mater. Sci. Lett.* **1** (1982) 211.
189. *Idem*, as [83], p. 145.
190. A. S. ARGON, G. W. HAWKINS and H. Y. KUO, *J. Mater. Sci.* **14** (1979) 1707.
191. L. ACKERMANN and P. FOURNIER, as [13], p. 1407.
192. R. B. POND, R. E. MARINGER and C. E. MOBLEY, in "New Trends in Materials Fabrication" (American Society for Metals, Metals Park, Ohio, 1976) p. 128.
193. F. C. HOLTZ and N. M. PARIKH, *Metal. Progr.* **90** (2) (1966) 117.
194. A. KASAK and E. J. DULIS *Powder Metall.* **21** (1978) 114.
195. *Idem, Engineer's Digest* **39** (6) (1978) 36.
196. C. WICK, *Manuf. Engng.* **85** (3) (1980) 52.
197. H. TAKIGAWA, H. MANTO, N. KAWAI and K. HOMMA, *Powder Metall.* **24** (1981) 196.
198. F. A. KIRK, *ibid.* **9** (1982) 198.
199. E. A. DICKINSON, *Metal Powder Rep.* **32** (2) (1977) 85.
200. R. J. CAUSTON and J. J. DUNKLEY, in "Hot-Working and Forming Processes" (The Metals Society, London, 1980) p. 244.
201. *Idem*, Proceedings of the 5th International Con-

ference on P/M, Czechoslovakia 1978, Part I, p. 265.
202. N. KAWAI and H. TAKIGAWA, *Metal Powder Rep.* **37** (1982) 237.
203. S. ASHLEY, *Amer. Metal Market Metalworking News* **89** No. 95 (1981) 14.
204. *Idem, ibid.* **89** No. 245 (1981) 13.
205. R. RAY, *J. Mater. Sci.* **16** (1981) 2924; 2927.
206. *Idem, Res. Mech. Lett.* **1** (1981) 261.
207. *Idem*, as [13], p. 1515.
208. *Idem*, as [83], p. 435.
209. *Idem, Mater. Sci. Eng.* **52** (1982) 85.
210. *Idem, Met. Progr.* **121** (1982) 29.
211. *Idem, Int. J. Powder Metall.* **18** (1982) 209.
212. *Idem, Metal Powder Rep.* **38** (1983) 47.
213. *Idem*, Marko Materials publicity leaflets received Jan. 1983.
214. R. W. CAHN, *Ann. Rev. Mater. Sci.* **12** (1982) 51.
215. W. A. GLAESER and B. P. FAIRAND, in "Wear of Materials", edited by K. C. Ludema *et al.*, (American Society of Mechanical Engineers, 1979) p. 304.
216. J. D. AYERS, T. R. TUCKER and R. J. SCHAEFER, as [9], p. 212.
217. R. J. SCHAEFER, T. R. TUCKER and J. D. AYERS, as [66], p. 754.
218. J. D. AYERS, R. J. SCHAEFER and W. P. ROBEY, *J. Metals* **33** (1982) 19.
219. J. C. BITTENCE, *Materials Engng.* **95** No. 4 (1982) 57.
220. B. G. LEWIS and P. R. STRUTT, *J. Metals* **34** (1982) 37.
221. S. P. MIDSON, R. A. BUCKLEY and H. JONES, as [13], p. 1521.
222. R. L. BICKERDIKE, W. N. MAIR, P. G. PARTRIDGE, H. C. RANSON, G. HUGHES, D. CLARK and J. N. EASTABROOK, US Patent 4033793 (1977).
223. R. G. BORDEAUX, C. ADAM and E. VAN REUTH, as [13], p. 155.
224. V. A. TRACEY and C. P. CUTLER, *Powder Metall.* **24** (1981) 32.
225. D. L. WILLIAMS, *ibid.* **20** (1977) 84.
226. P. WILDGOOSE, N. G. TURNER, H. F. DAVIES, B. J. HELLIWELL, R. UBANK and H. HARRISON, *ibid.* **24** (1981) 75.
227. R. J. PATTERSON, A. R. COX and E. C. VAN REUTH, *J. Metals* **39** (1980) 34.
228. R. J. PATTERSON, A. R. COX, T. D. TILLMAN and E. C. VAN REUTH, as [9], p. 416.
229. N. J. de CRISTOFARO and C. HENSHEL, *Welding J.* **57** (1978) 33.
230. *Idem*, US Patent 4182628 (1980).
231. T. L. D'SILVA, US Patent 4182628 (1980).
232. J. MEGUSAR, L. ARNBERG, J. B. VANDERSANDE and N. J. GRANT, *J. Nucl. Mater.* **99** (1981) 190.
233. (a) E. TESTART, J. MEGUSAR, L. ARNBERG and N. J. GRANT, *ibid.* **103/104** (1981) 833; (b) J. MEGUSAR, O. K. HARLING and N. J. GRANT, *ibid.* **103/104** (1981) 961; (c) L. ARNBERG, J. MEGUSAR, D. IMESON, H. J. FROST, J. B. VANDERSANDE, O. K. HARLING and N. J. GRANT, *ibid.* **103/104** (1981) 1005; (d) L. ARNBERG, J. B. VANDERSANDE, H. J. FROST and O. K. HARLING, *ibid.* **103/104** (1981) 1069; (e) J. MEGUSAR, L. ARNBERG, J. B. VANDERSANDE and N. J. GRANT, *ibid.* **103/104** (1981) 1103.
234. N. J. GRANT, J. MEGUSAR and L. ARNBERG, as [13], p. 1491.
235. J. MEGUSAR, L. ARNBERG, J. B. VANDERSANDE and N. J. GRANT, *J. Nucl. Mater.* **103/104** (1981) 1109.
236. J. F. WOOLDRIDGE and J. A. EASTON, *Industrial Heating* **45** No. 4 (1978) 44.
237. M. NAKA, K. HASHIMOTO and T. MASUMOTO, *J. Jpn Inst. Metals* **38** (1974) 835.
238. *Idem, Corrosion* **32** (1976) 146.
239. T. MASUMOTO and K. HASHIMOTO, *J. Physique* **41** (Suppl. 8) (1980) C8-894.
240. L. B. JOHNSON, H. OTANI, M. J. NEARY, J. W. HAUCK, T. M. HEAVEN and R. J. REGENITTER, *J. Biomech. Mater. Res.* 8 (1974) 3.
241. J. V. WOOD and S. C. KING, *J. Mater. Sci.* **13** (1978) 1119.
242. G. FANINGER, D. MERZ and H. WINTER, in "Rapidly Quenched Metals", edited by N. J. Grant and B. C. Giessen (MIT Press, Cambridge, MA, 1976) p. 483.
243. E. R. SLAUGHTER and S. K. DAS, as [9], p. 354.
244. A. N. PATEL, L. F. VASSAMILLET and A. H. CLAVER, as [83], p. 259.
245. G. J. YUREK, D. EISEN and A. GARRATT-REED, *Met. Trans. A* **13A** (1982) 473.
246. T. TSURU, S. X. ZHANG and R. M. LATANISION, as [13], p. 1437.
247. T. R. ANTHONY and H. E. CLINE, *J. Appl. Phys.* **49** (1978) 1248.
248. C. W. DRAPER, R. E. WOODS and L. S. MEYER, *Corrosion* **36** (1980) 405.
249. K. ASAMI, T. SATO, K. HASHIMOTO, T. SHIGEMATSU and S. KIMURA, as [13], p. 177.
250. R. B. DIEGLE, *SAMPE Q.* **13** (1982) 26.
251. A. YOKOHAMA, H. KOMIYAMA, H. INOUE, T. MASUMOTO and H. M. KIMURA, *Scripta Metall.* **15** (1980) 365.
252. H. KOMIYAMA, A. YOKOYAMA, H. INOUE, T. MASUMOTO and H. KIMURA, in "Structure and Properties of Amorphous Metals II", Suppl. to *Sci. Rep. RITU* **A28** (1980) 217.
253. A. YOKOHAMA, H. KOMIYAMA, H. INOUE, T. MASUMOTO and H. M. KIMURA, as [13], p. 1419.
254. A. KAWASHIMA and K. HASIMOTO, as [13], p. 1427.
255. M. HARA, K. HASHIMOTO and T. MASUMOTO, as [13], p. 1423.
256. C. S. BROOKS, F. D. LEMKEY and G. S. GOLDEN, as [83], p. 397.
257. A. J. MAELAND, in "Hydrides for Energy Storage", edited by A. F. Anderson and A. J. Maeland (Pergamon, Oxford, 1978) p. 447.
258. A. J. MAELAND, L. E. TANNER and G. G. LIBOWITZ, *J. Less Common Metals* **74** (1980) 279.
259. F. H. M. SPIT, J. W. DRIJVER and S. RADELAAR, *Z. Physik. Chem.* **116** (1979) 225.
260. *Idem, Scripta Metall.* **14** (1980) 1071.
261. F. H. M. SPIT, J. W. DRIJVER, W. C. TURKENBERG and S. RADELAAR, *J. Physique* **41** (Suppl. 8) (1980) C8-890.

262. F. SPIT, K. BLOK, E. HENDRIKS, G. WINKELS, W. TURKENBERG, J. W. DRIJVER and S. RADELAAR, as [13], p. 1635.
263. K. AOKI, A. HORATA and T. MASUMOTO, *Sci. Rep. RITU* **A29** (1981) 218.
264. *Idem*, as [13], p. 1649.
265. P. DUWEZ and S. C. H. LIN, *J. Appl. Phys.* **38** (1967) 4096.
266. F. E. LUBORSKY, in "Amorphous Magnetism", edited by R. A. Levy and R. Hasegawa (Plenum, New York, 1977) p. 345.
267. F. E. LUBORSKY, J. J. BECKER, P. G. FRISCHMANN and L. A. JOHNSON, *J. Appl. Phys.* **49** (1978) 1769.
268. F. E. LUBORSKY and L. A. JOHNSON, *J. Physique* **41** Colloq. C8 (1980) C8-820.
269. L. I. MENDELSOHN, E. A. NESBITT and G. R. BRETTS, *IEEE Trans. Mag.* **Mag-12** (1976) 924.
270. L. I. MENDELSOHN and E. A. NESBITT, US Patent 4030892 (1977).
271. H. WARLIMONT and R. BOLL, *J. Mag. Mater.* **26** (1982) 97.
272. K. HIROTA, private communication to H. S. Chen and K. A. Jackson, as [73], p. 255.
273. Anon., in "Amorphous and Metastable Microcrystalline Rapidly Solidified Alloys: Status and Potential", US National Materials Advisory Board Report 358 (1980) Ch. 12.
274. N. TSUYA, K. I. ARAI, K. OHMORI, H. SHIMANAKA and T. KAN, *IEEE Trans. Mag.* **Mag-16** (1980) 728.
275. J. J. GILMAN, *Physics Today* **28** No. 5 (1975) 46.
276. C. C. TSUEI and P. DUWEZ, *J. Phys. E: Sci. Instrum.* **4** (1971) 466.
277. R. HASEGAWA and L. E. TANNER, *J. Appl. Phys.* **48** (1977) 3211.
278. T. NAOHARA, A. INOUE, T. MASUMOTO and K. KUMADA, as [13], p. 1581.
279. *Idem, Met. Trans. A* **13A** (1982) 337.
280. H. HEINRICH, T. HAAG and G. GEIGER, *J. Phys. D: Appl. Phys.* **11** (1978) 2439.
281. H. WARLIMONT, *Physics in Technology* **11** (1980) 28.
282. W. L. JOHNSON, in "Glassy Metals I", edited by H. J. Guntherodt and H. Beck (Springer-Verlag, Berlin, 1981) p. 191.
283. A. INOUE, A. HOSHI, C. SURYANARAYANA and T. MASUMOTO, *Scripta Metall.* **14** (1980) 1077.
284. A. INOUE, Y. TAKAHASHI, A. HOSHI, C. SURYANARAYANA and T. MASUMOTO, *J. Appl. Phys.* **52** (1981) 4711.
285. A. INOUE, A. HOSHI, C. SURYANARAYANA and T. MASUMOTO, as [13], p. 1249.
286. G. MANFRÉ, G. SERVI and C. RUFFINO, *J. Mater. Sci.* **9** (1974) 74.
287. G. MANFRÉ and G. SERVI, *Wire Industry* **42** (1975) 281.
288. V. K. SARIN and N. J. GRANT, *Met. Trans.* **3** (1972) 875.
289. *Idem, Powder Metall Int.* **11** (1979) 153.
290. H. C. CHIA and A. STARKE, *Wire J.* **12** No. 6 (1979) 66.
291. J. C. NICOUD, US Patent 4127426 (1978).
292. R. MEHRABIAN, as [7], p. 9.
293. J. A. HORWATH and L. F. MONDOLFO, *Acta Metall.* **10** (1962) 1037.
294. B. P. BARDES and M. C. FLEMINGS, *Trans. Amer. Foundrymen's Soc.* **74** (1966) 406.
295. G. R. ARMSTRONG and H. JONES, as [127], p. 454.
296. V. K. SARIN and N. J. GRANT, *Met. Trans.* 8 (1972) 875.
297. W. E. BROWER, R. STRACHAN and M. C. FLEMINGS, *Cast Met. Res. J.* **6** (1970) 176.
298. P. A. JOLY and R. MEHRABIAN, *J. Mater. Sci.* 9 (1974) 1446.
299. J. I. NURMINEN and H. D. BRODY, in "Titanium Science and Technology", edited by R. I. Jaffee and H. M. Burte (Plenum, New York, 1973) p. 1893.

Received 1 April
and accepted 26 April 1983